Pergamon

PII: S0191–8141(98)00005–4

Journal of Structural Geology, Vol. 20, No. 6, pp. 745 to 764, 1998

0191-8141/98 $19.00 + 0.00

Mid- to Late Cretaceous ductile deformation and thermal evolution of the crust in the northern Dome Rock Mountains, Arizona

STEFAN S. BOETTCHER* and SHARON MOSHER

Department of Geological Sciences, University of Texas at Austin, Austin, TX 78712, U.S.A.

(*Received* 6 *May* 1997; *accepted in revised form* 19 *December* 1997)

Abstract—Mid- to Late Cretaceous basement-involved deformation in the Maria Tectonic Belt of southeastern California and west-central Arizona varies in style from low-angle overthrusts to km-scale fold nappes. To establish the relationship between tectonite fabrics and thermal evolution of the rocks, structural and petrographic analysis was conducted in the northern Dome Rock Mountains, where the two different styles converge. A penetrative northeast-dipping foliation forms the most conspicuous fabric in an ~5 km wide zone of distributed ductile deformation. Within the broader zone of ductile deformation, northeast-dipping shear zones contain evidence for both southwest- and northeast-directed deformation. Textural analysis of mylonitic rocks reveals that southwest-directed deformation occurred under prograde conditions, whereas northeast-directed deformation occurred under retrograde conditions. Southwest-directed deformation resulted in tubular (extreme sheath) fold development on a kilometer scale in the footwall of a reverse-sense shear zone. Northeast-directed deformation cuts the map-scale tubular fold and is inferred to have developed as a manifestation of gravitational collapse of rocks mechanically weakened by fluid infiltration and upper greenschist- to lower amphibolite-facies metamorphism. We propose that the mode and degree of fluid infiltration, rather than temperature or structural level alone, controlled the style of deformation in the Maria Belt. © 1998 Elsevier Science Ltd. All rights reserved

INTRODUCTION

Mid- to Late Cretaceous ductile deformation and greenschist- to amphibolite-facies metamorphism affected the Maria Tectonic Belt, an ~9,000 km^2 area in southeastern California and west-central Arizona (Fig. 1). This deformation occurred during the time of the Sevier (D_2, ~115–80 Ma) and Laramide orogenies (D_3, ~80–55 Ma) and is superposed on preexisting Jurassic (?) structures (D_1) (Haxel *et al.*, 1984; Reynolds *et al.*, 1986; Dickinson *et al.*, 1986; Laubach *et al.*, 1989). On the eastern side of the belt, in the Harquahala, Little Harquahala, and Granite Wash Mountains, Proterozoic and Jurassic crystalline rocks are thrust up to several tens of kilometers across steeply-dipping Paleozoic cratonic metasedimentary rocks and the Jurassic and Cretaceous McCoy Mountains Formation. Gently dipping faults and parallel mylonitic shear zones contain kinematic indicators such as winged augen, *S–C* fabrics, and en échelon veins that indicate top-to-the-southwest shear during thrust-sense deformation (Laubach, 1986; Richard, 1988; Laubach *et al.*, 1989; Marin, 1993). Towards the west, in the Big and Little Maria Mountains, shearing on the inverted limbs of km-scale southwest-facing synclines resulted in attenuation of the entire Paleozoic cratonal section to as little as 1% of its original thickness (~1 km) without loss of continuity of stratigraphic sequence (Hamilton, 1982, 1987). Thrust faults are rarely observed and the majority of shortening is thought to have been accommodated by folding, limb attenuation, and crystal-plastic deformation in mylonitic shear zones. Shear zone fabrics associated with crustal shortening are typically symmetrical, with few grain-scale indicators of southwest-directed shearing (Ballard, 1990). Unlike the eastern part of the belt, southwest-directed fabrics are reactivated in northeast-directed, extensional shear zones that developed during regional cooling (Ballard, 1990).

The goal of this paper is to document the style, kinematics, and magnitude of strain related to mid- to Late Cretaceous ductile deformation in the northern Dome Rock Mountains, Arizona and place deformation fabrics in the context of the thermal evolution of the crust. Because of the excellent exposure of layered Paleozoic metasedimentary rocks, lack of major Tertiary extensional structures, and geographic position near the center of the Maria Belt, the northern Dome Rock Mountains are an important locality for addressing the variation in style of mid- to Late Cretaceous strain across the belt. Petrographic study and microtextural analysis of tectonite fabrics are used to establish the relationship between metamorphism and deformation during the Late Cretaceous transition from southwest-directed shortening to northeast-directed extension. Field mapping at 1:6000 and geometric analysis are used to define a tubular fold (extreme sheath fold) geometry on a kilometer scale and estimate the magnitude of shear strain in the footwall of a Mesozoic shear zone.

*Present address: Exxon Production Research Company, P.O. Box 2189, Houston TX 77027, U.S.A. (ssboett@epr.exxon.com).

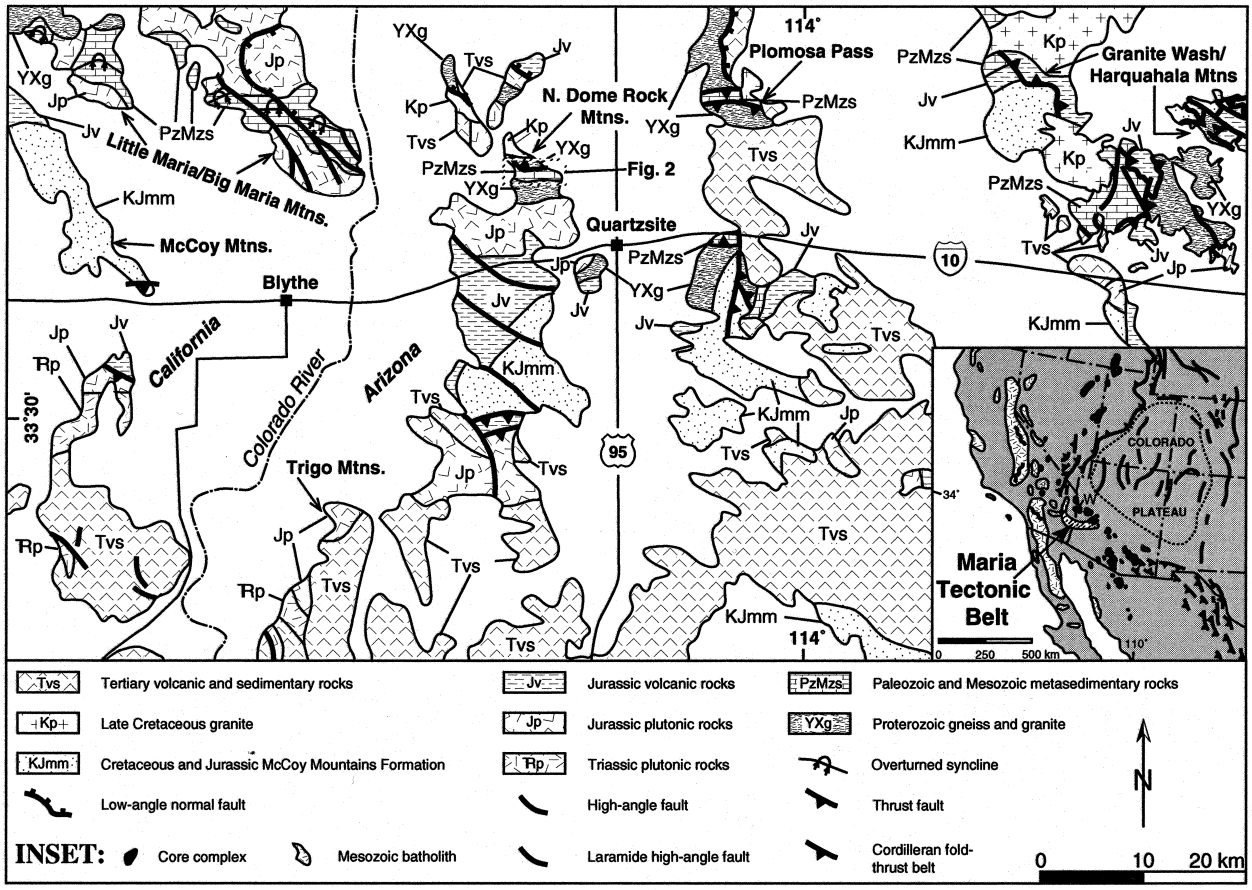

Fig. 1. Generalized geologic map of the central segment of the Maria Tectonic Belt (Modified from Tosdal, 1990). Inset shows geographic position of the Maria Tectonic Belt relative to other major structures of the Cordilleran orogen; W–Whipple Mountains (modified from Haxel *et al.*, 1984).

GEOLOGIC FRAMEWORK

The northern Dome Rock Mountains are part of a ~50 km wide, stable block of pre-Tertiary igneous and metasedimentary rocks between the Colorado River extensional corridor (Howard and John, 1987) to the northeast and a region of upper crustal extension to the southwest (Sherrod and Tosdal, 1991; Spencer and Reynolds, 1991) (Fig. 1). The range is not internally dismembered or underlain by Tertiary extensional faults or ductile shear zones. In the mountain pass area known as Boyer Gap (Fig. 2; Yeats, 1985; Boettcher, 1996), an arcuate belt of polydeformed upper greenschist to lower amphibolite facies metasedimentary rocks and nonconformably underlying ~1400 Ma megacrystic, K-feldspar augen gneiss are intruded by Jurassic granitoids (Jp—Fig. 1; Jlg, Jg—Fig. 2) of the Kitt Peak–Trigo Peaks super-unit (Tosdal *et al.*, 1989). Three discrete, separable phases of ductile deformation affected the rocks in this area (Boettcher, 1996) and are summarized below.

D_1 produced a >2 km scale, north- to northwest-facing recumbent syncline (F_1) and penetrative foliation (S_1) during late Middle Jurassic magmatism. The formation, timing and tectonic significance of this fold are discussed in Boettcher (1996), however, its orientation and geometry have a major influence on the subsequent (D_2–D_3) structures, the focus of this paper.

D_2 produced ductile shear zones and thrust faults with top-to-the-southwest motion, a regionally extensive tubular (extreme sheath) fold, south- to southwest-vergent folds (F_2), sheath folds, and a penetrative foliation (S_2) during mid- to Late Cretaceous crustal shortening. The northernmost D_2 structure is the Tyson thrust (Yeats, 1985; Boettcher, 1996), which superposes Proterozoic augen gneiss (~1400 Ma, U/Pb zircon, Tosdal, personal communication, 1993) on Triassic metasedimentary rocks and is cross-cut by a granitic stock of Late Cretaceous age (Tyson Wash granite, ~86 Ma, $^{206}Pb/^{238}U$ sphene, Tosdal, personal communication, 1993; Kp in northern Dome Rock Mountains—Fig. 1). In the hangingwall, the entire exposure of Proterozoic gneiss is mylontized. In the footwall, a broad zone of distributed deformation extends ~5 km south of the thrust, up to the northern margin of the Middle Jurassic Middle Camp granodiorite pluton (165 ± 2 Ma, U/Pb zircon, Tosdal *et al.*, 1989; Jp in northern Dome Rock Mountains—Fig. 1). Within the broad zone, the most conspicuous fabric is a penetrative northeast-dipping schistosity (S_2) parallel to mylonitic foliation in the hangingwall. The foliation is parallel to the axial planes of cm- to km-scale, south-

west-vergent, tight to isoclinal folds (F_2) of a pre-existing foliation (S_1) in metasedimentary rocks and middle Jurassic diorite and granodiorite. These folds (F_2) are superposed on the >2 km-scale north- to northwest-facing recumbent syncline (F_1), resulting in a composite fold nappe with a tubular (extreme sheath) geometry that is best observed in Paleozoic metasedimentary rocks (Figs 2 & 3). Syn-metamorphic faults disrupting the stratigraphic succession of Paleozoic units occur at low angles to stratigraphic contacts and are interpreted to have developed during extreme attenuation of limbs during folding. Also found within this broad zone are northeast-dipping, spaced, ductile shear zones with mylonitic fabrics parallel to S_2, including the Tung Hill shear zone, which has been reactivated during D_3, and the Boyer Gap shear zone, which occurs within Jurassic and Proterozoic augen gneiss (Yeats, 1985; Boettcher, 1996) (Fig. 2). The shear zones, S_2 foliation, F_2 folds, and modification of F_1 folds are inferred to have formed synchronously during D_2, top-to-the-southwest shearing along the Tyson thrust.

D_3 resulted in northeast-vergent folds (F_3), non-penetrative foliation (S_3) and reactivation of D_2 shear zones during Late Cretaceous to early Tertiary exhumation. Unlike D_1 and D_2 structures, D_3 structures occur in discrete zones and are not penetrative at the scale of the mountain range. F_3 folds within these zones are cm- to tens of m-scale, northeast-vergent folds of S_2, and spaced S_3 cleavages cut earlier fabrics. The Tung Hill, Boyer Gap and Tyson thrust shear

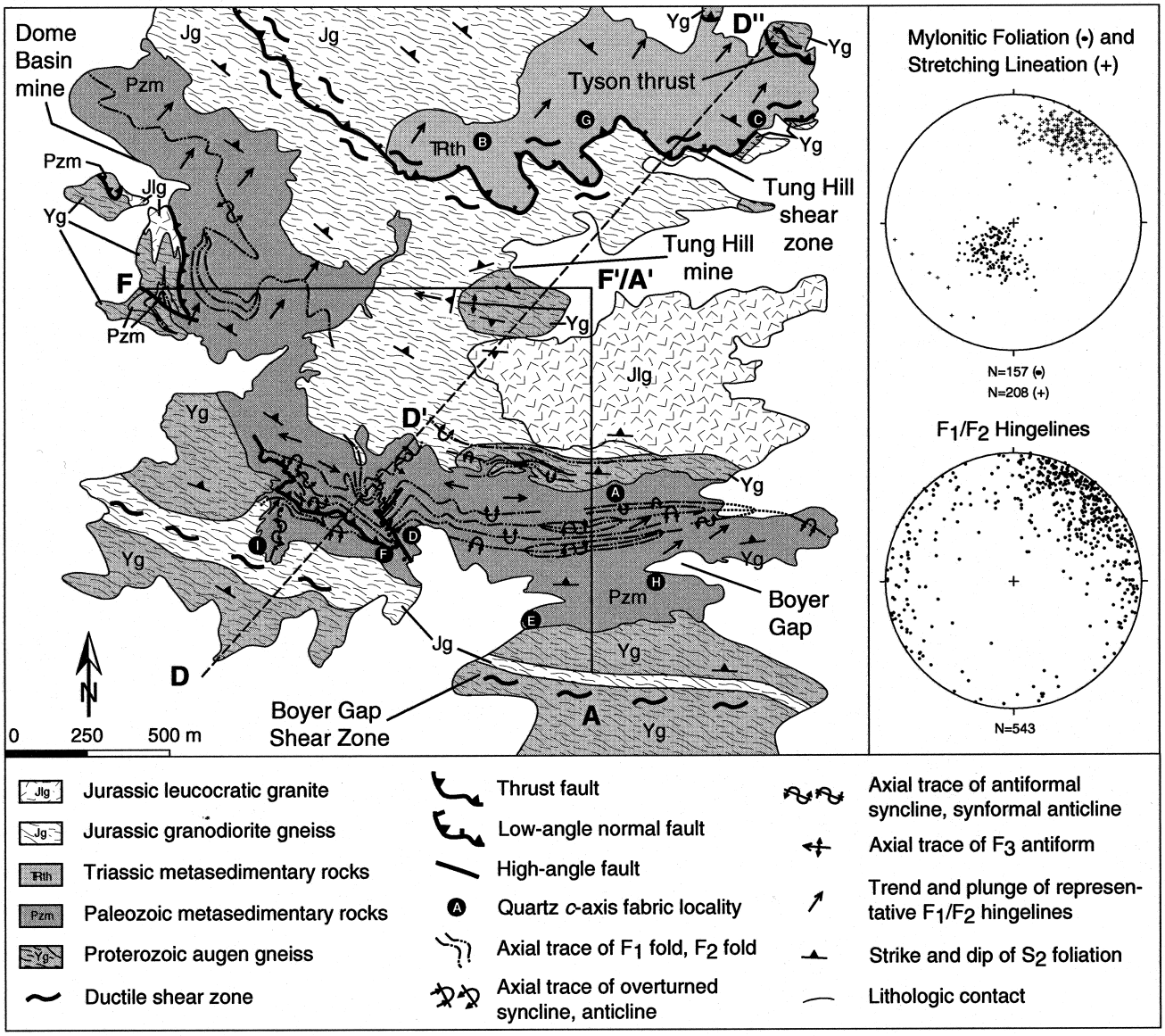

Fig. 2. Map showing principal structural elements in the northern Dome Rock Mountains. From Boyer Gap to the Dome Basin mine area, the map-scale outcrop pattern in Paleozoic metasedimentary rocks is controlled by a series of asymmetric, south- to southwest-verging anticlines and synclines with wavelengths of tens to hundreds of meters. These second phase folds (F_2) are superposed on an earlier north- to northwest-facing recumbent syncline (F_1), resulting in both upward- and downward-facing folds. D–D'', A–A'/F–F designates cross section lines for Fig. 3. Stereonets are equal-area lower hemisphere projections.

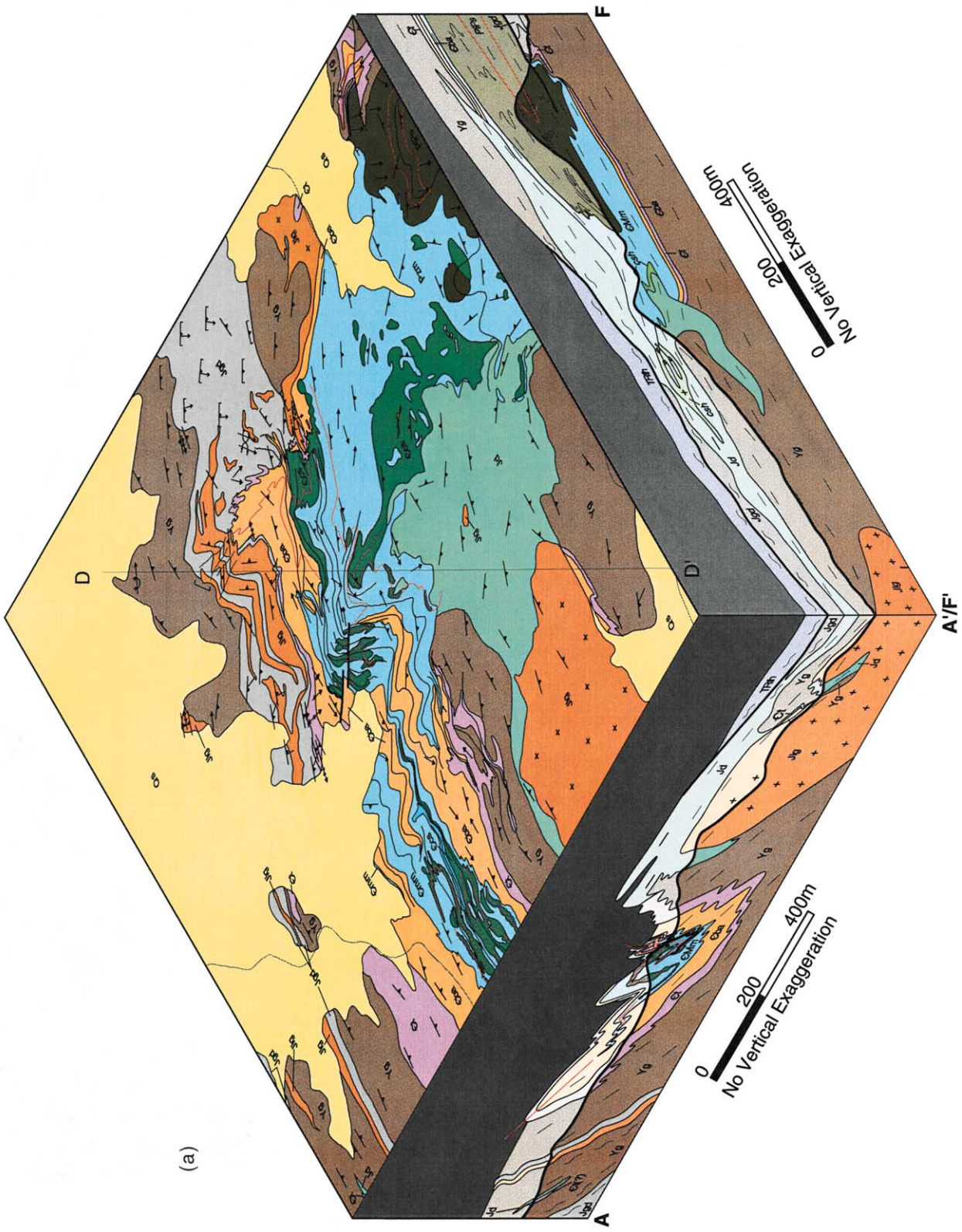
(a)
D
D'
F
A
A'/F'
No Vertical Exaggeration
0
200
400m
No Vertical Exaggeration
0
200
400m

Fig. 3(a).

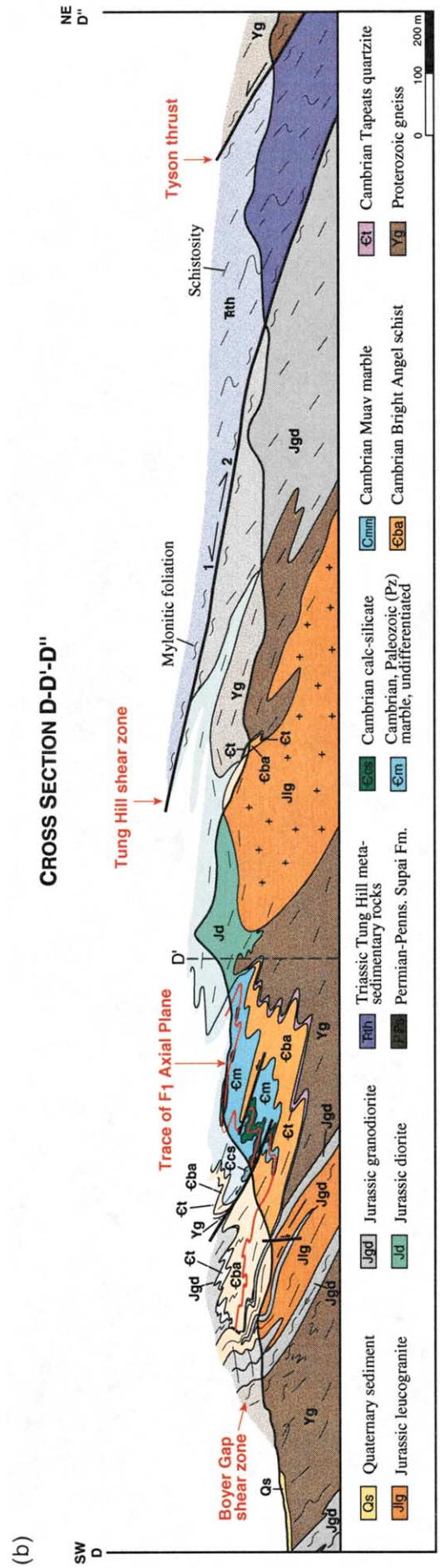

Fig. 3. (a) Isometric projection shows three-dimensional view of composite structure in the northern Dome Rock Mountains. View is to the southwest, parallel to D_2 transport direction. Units with light shading in cross sections are above topography and are projected along strike or up dip. Grey shading is projection space between map view and cross sections. (b) Cross section D–D'–D'' shows profile view of composite F_1/F_2 fold nappe in the footwall of the Tyson thrust. Nappe is cut by D_3 normal fault (Tung Hill shear zone) that resulted in translation of Triassic Tung Hill metasedimentary rocks down to the northeast from an original position in the core of the nappe. Lighter shades shown above topography to denote projection along trend or down plunge of composite structure. For location, see Fig. 2.

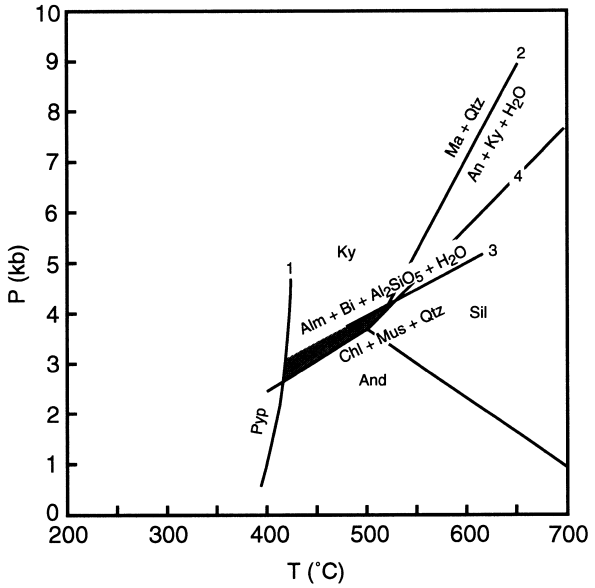

Fig. 4. Metamorphic reactions defining possible pressure–temperature space during M_2 metamorphism: (1) Pyrophyllite = Quartz + Kyanite (Kerrick, 1968); (2) Margarite + Quartz = Anorthite + Kyanite + Water (Storre and Nitsch, 1974); (3) Chlorite + Muscovite + Quartz = Almandine + Biotite + Kyanite + Water (Hirschberg and Winkler, 1968); (4) Andalusite = Kyanite; Kyanite = Sillimanite (Holdaway, 1971). In addition, the presence of wollastonite in calc-silicate rocks of the Supai Formation is indicative of temperatures greater than 450°C at pressures greater than ~2.5 kb (Greenwood, 1976).

zones contain kinematic evidence for late-reactivation during northeast-directed, normal-sense shear. Along the Tung Hill shear zone, normal-sense shear (D_3) resulted in juxtaposition of Triassic metasedimentary rocks directly over mylonitic augen gneiss with a U/Pb zircon age of 1410 ± 3 Ma (Boettcher, 1996) (Fig. 2). The Tyson thrust is the only structural discontinuity in the northern part of the range with preserved older on younger thrust-sense juxtaposition. In addition to kinematic analysis, the relationship between metamorphism and fabric development provides a key for distinguishing northeast-directed fabrics (D_3) from southwest-directed fabrics (D_2) and establishing the kinematics of each phase of deformation.

MID- TO LATE CRETACEOUS METAMORPHISM

Mineral assemblages in calc-silicate rocks, marbles, and calcareous and pelitic schists, described below, place constraints on the pressure–temperature conditions during peak mid- to Late Cretaceous metamorphism (Fig. 4). In metasedimentary rocks, an upper greenschist- to lower amphibolite-facies metamorphic assemblage overprints an earlier metamorphic fabric (S_1, M_1) defined by aligned relict muscovite and pressure-solution seams (Boettcher, 1996). The second metamorphic assemblage (M_2) is defined by minerals that grew both parallel to and across S_2 foliation, indicating that M_2 metamorphism outlasted D_2 deformation.

Calc-silicate rocks consist of calcite + quartz + epidote + biotite + K-feldspar ± diopside ± plagioclase. Diopside occurs in distinct compositional bands parallel to S_2 foliation. Above the basal calc-silicate unit in the Supai Formation, sharply defined 0.1 mm to 1 m layers of nearly 100% wollastonite occur between layers of quartzite (Fig. 5a). The wollastonite shows a dimensional preferred orientation parallel to layer margins and S_2 foliation outside of the layers and is also observed in fractures that cut across S_2 foliation. Calcite, quartz, and wollastonite grains are not observed where all three minerals are in contact, indicating the reaction $CaCO_3 + SiO_2 = CaSiO_3 + CO_2$ locally proceeded to completion upon loss of either quartz or calcite reactants.

Numerous small (1 m^2) to large (tens of m^2) bodies of calc-silicate hornfels and granofels are present at Cambrian schist/marble contacts and within Cambrian calc-silicate rocks. These bodies typically consist of quartz + epidote + biotite + K-feldspar dominated hornfels and granofels. Irregularly shaped patches of coarse calcite and biotite are common in calc-silicate granofels and adjacent schist. Other minerals in granofels include randomly oriented tremolite, microcline, plagioclase, diopside, grossular, and magnetite. Veins of fibrous tremolite and actinolite, up to 15 cm wide, cut S_2 foliation in calc-silicate rocks.

The assemblage calcite + muscovite + clinochlore ± epidote ± quartz ± actinolite is typical of micaceous marbles. In Cambrian Muav marble, fine-grained needles of pale green actinolite form discontinuous and convolute pods that are surrounded by recrystallized calcite. Clinochlore is preserved as thin sheets on weathered S_2 foliation surfaces.

The M_2 metamorphic assemblage in calcareous schists of the Bright Angel Formation and Tung Hill metasedimentary rocks is characterized by the presence of quartz + muscovite + biotite + epidote ± plagioclase ± tourmaline. Elongate blades of muscovite, biotite and epidote are parallel to the axial planes of southwest-vergent folds and define S_2 foliation. M_2 epidote has been stretched along prominent basal parting planes. No garnet was observed in either formation, although garnet is present in the Bright Angel Formation ~125 km to the northwest in the Old Woman Mountains and Piute Range, California, where pressures were higher during mid- to Late Cretaceous metamorphism (Hoisch *et al.*, 1988).

North of the Tung Hill mine (Fig. 2), pelitic schist containing kyanite porphyroblasts up to 1 cm wide occurs as discontinuous 5–15 m layers within the Tung Hill metasedimentary rocks. The M_2 metamorphic mineral assemblage in these rocks is characterized by quartz + muscovite + kyanite + margarite ± chlorite ± feldspar. Margarite is interlayered with muscovite

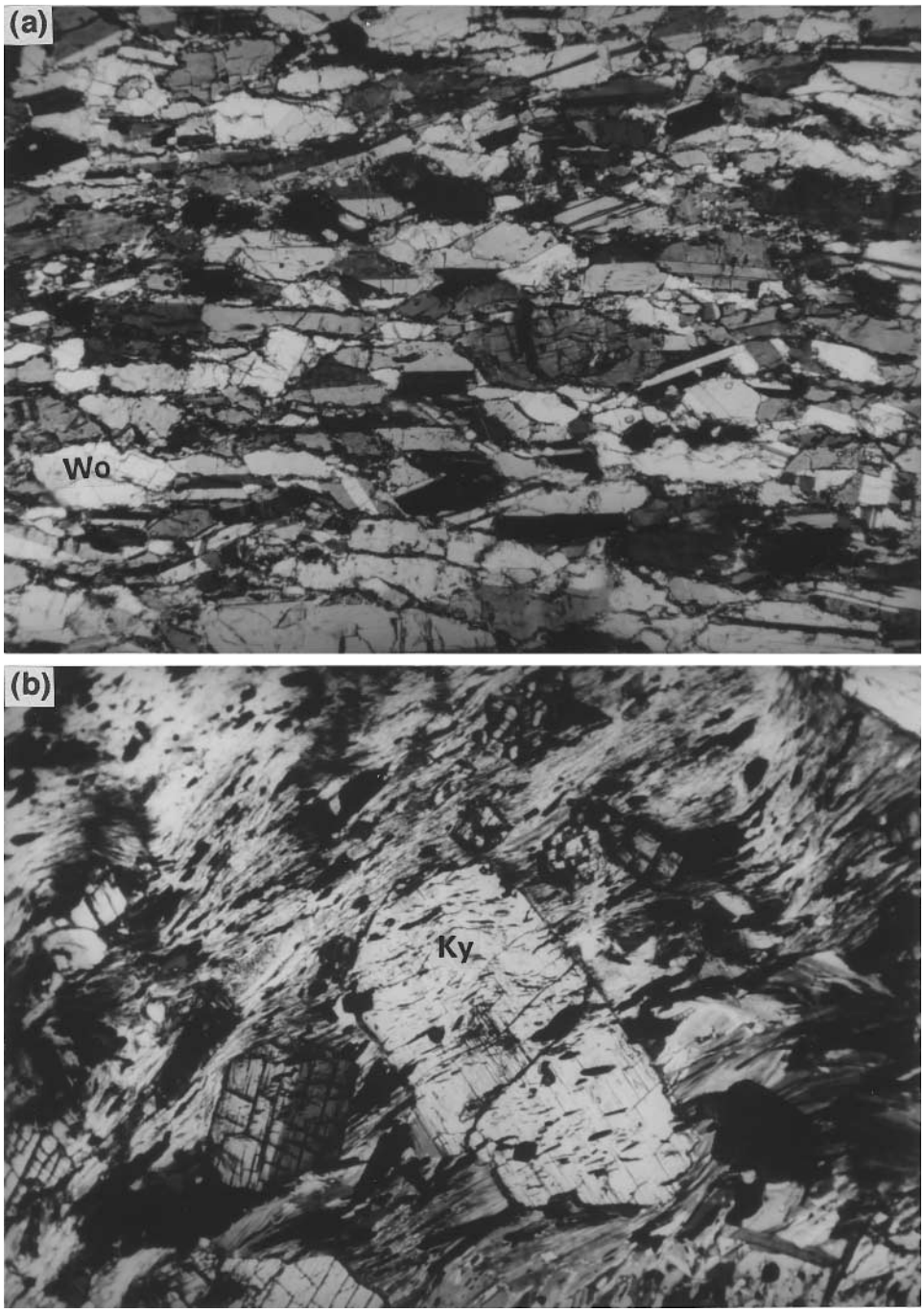

Fig. 5. (a) Photomicrograph of wollastonite (Wo) layer in calc-silicate gneiss from Pennsylvanian–Permian Supai Formation. Crossed polars, field of view is 1.7 mm. (b) Photomicrograph of kyanite (Ky) porphyroblasts in Triassic schist. Foliation defined by inclusion trails in porphyroblast is concordant with S_2 foliation in the matrix, indicating growth of the porphyroblast after development of the foliation. Crossed polars, field of view is 1.7 mm.

parallel to S_2 foliation; both are commonly crenulated. Kyanite occurs both parallel and oblique to the S_2 foliation, indicating that it continued to form after the cessation of D_2 deformation. Opaque inclusion trails in obliquely-oriented kyanite porphyroblasts are commonly straight and continuous with the external S_2 foliation (Fig. 5b); less commonly, they are discontinuous and curved. In one location, a 0.1–0.5 m wide quartz vein contains blades of aligned kyanite up to 5 cm long. The adjacent schist is dominated by randomly oriented kyanite porphyroblasts that overgrow S_2 foliation.

Mineral assemblages present in the metasedimentary rocks place constraints on the possible range of peak pressure–temperature conditions during M_2 metamorphism (Fig. 4). The assemblages quartz + muscovite + chlorite and quartz + margarite, presence of kyanite and wollastonite, and absence of garnet limits the range of possible temperature and pressure during peak metamorphism to ~450–515°C and ~2.5–4.1 kb.

The position of reaction 3 in Fig. 4, used here to provide an upper limit on pressure, is, however, a sensitive function of bulk composition. The location of this reaction corresponds to a typical $Fe^{2+}/(Fe^{2+}+Mg)$ ratio in pelitic rock of 0.8; if this ratio were lower, the reaction would move to pressures as much as 2 kb higher (Hirschberg and Winkler, 1968). The common occurrence of epidote, diopside, wollastonite and kyanite is consistent with lower amphibolite-facies metamorphism. However, the lack of staurolite in rocks where chlorite and muscovite are in contact is suggestive of upper greenschist facies metamorphism (Winkler, 1979). The presence of extension fractures filled with minerals that formed under upper greenschist- to lower amphibolite-facies conditions (kyanite, tremolite, actinolite) is indicative of high fluid pressure during at least part of the metamorphism (Etheridge *et al*., 1984).

SHEAR ZONE FABRICS

Mylonitic rocks in the hangingwall of the Tyson thrust, near the Tung Hill Mine in the Tung Hill shear zone, on the south side of Boyer Gap in the Boyer Gap shear zone, and within Jurassic igneous rocks as far south as Marquita Pass (Figs 1 & 2) contain evidence for both southwest- and northeast-directed deformation. Although shear zone fabrics are dominated by D_3 northeast-directed kinematic indicators, they contain evidence for an earlier phase of southwest-directed shearing (D_2) that is interpreted to be coeval with the formation of southwest-verging folds.

In metaigneous rocks, the S_2 foliation becomes mylonitic in 10–100-m-thick, northeast-dipping shear zones. The change from distributed protomylonitic fabric to discrete zones of mylonite and ultramylonite is characterized by reduction in grain size of feldspar megacrysts to less than one centimeter in diameter, decrease in spacing of foliation planes to less than one centimeter, and parallelism of foliation planes. Mylonitic foliation (290°, 30° NE) in the hangingwall of the Tyson thrust, the Boyer Gap shear zone, and the Tung Hill shear zone parallels the S_2 schistosity in metasedimentary rocks (Fig. 2); both cross-cut steeply-dipping S_1 foliation. Streaks of stretched feldspar and aggregates of quartz and biotite are up to 20 cm long and form a northeast-trending (20°, 031°), down-dip elongation lineation (Fig. 2). The largely orthorhombic fabrics in D_2 mylonitic rocks, relatively planar lithologic layer contacts on limbs of major structures, occurrence of tubular folds (Fig. 6a), and penetrative foliation suggest a generally non-coaxial strain path with a component of coaxial flattening strain.

Evidence for an early phase of high-temperature mylonitization is preserved by S_2 mylonitic foliation at the base of the Boyer Gap shear zone. Dynamically recrystallized quartz and feldspar and dimensionally-oriented biotite form type I *S–C* mylonite (Lister and Snoke, 1984) in sheared Proterozoic gneiss and indicate top-to-the-southwest shear (Fig. 6b). In thin section, feldspar forms relatively large (~70 μm diameter), nearly equigranular dynamically recrystallized grains with straight grain boundaries. Rare relict porphyroclasts are well recovered, contain subgrains, and have myrmekite on their margins. Surrounding the relict porphyroclasts, and forming a rough outline of pre-existing larger grains when viewed in plane light, are grains of similar size and shape as subgrains and recrystallized matrix grains. Recrystallized quartz and feldspar grains occur in anastomosing bands surrounding relict feldspar porphyroclasts. These textures all indicate that rotation recrystallization (Poirer, 1985, p. 181) was the dominant mechanism of feldspar recrystallization, requiring temperatures greater than 450°C (Fitz Gerald and Stünitz, 1993).

Quartzites and marbles in Boyer Gap also show evidence for high-temperature dynamic recrystallization during D_2. Quartz grains in quartzite with D_2 mylonitic fabric exhibit only minor continuous undulatory extinction and are essentially strain-free (Fig. 6c). Inclusions of tourmaline and muscovite aligned parallel to S_2 within equigranular quartz grains are evidence for an early phase of 'fast' grain-boundary migration and indicate that highly mobile grain boundaries were able to overcome the pinning effects of these phases during dynamic recrystallization (cf. Urai *et al*., 1986). Subgrains in relict larger grains with a similar size and shape as equigranular new grains indicate rotation recrystallization occurred after grain boundary migration, reducing the grain size and obscuring evidence of the earlier process. The local occurrence of equilibrium grain boundary textures is evidence for some surface energy-driven grain boundary migration concurrent with or subsequent to rotation recrystallization. In marble, calcite crystals are elongate parallel to S_2 with long dimension generally less than ~0.5 mm. Multiple sets of planar twin lamellae are common and recrystallized grains have relatively uniform extinction and grain size.

D_2 deformation is recorded in mylonites by penetrative S_2 foliation and stretching lineation. A strong crystallographic preferred orientation is associated with this deformation. The high degree of recovery and rotation recrystallization of feldspar and presence of myrmekite in metaigneous rocks is consistent with the 450°C–515°C estimate of peak temperature derived from the M_2 metamorphic mineral assemblage (cf. Fitz Gerald and Stünitz, 1993). The change from high-temperature (>450°C) 'fast' grain-boundary migration in quartz, indicated by inclusions defining S_2 foliation, to rotation recrystallization, could reflect either a modest decrease in temperature, an increase in strain rate, a decrease in volume of fluids, or some combination of these factors (cf. Urai *et al*., 1986). The textural evidence for M_2 metamorphism outlasting D_2 defor-

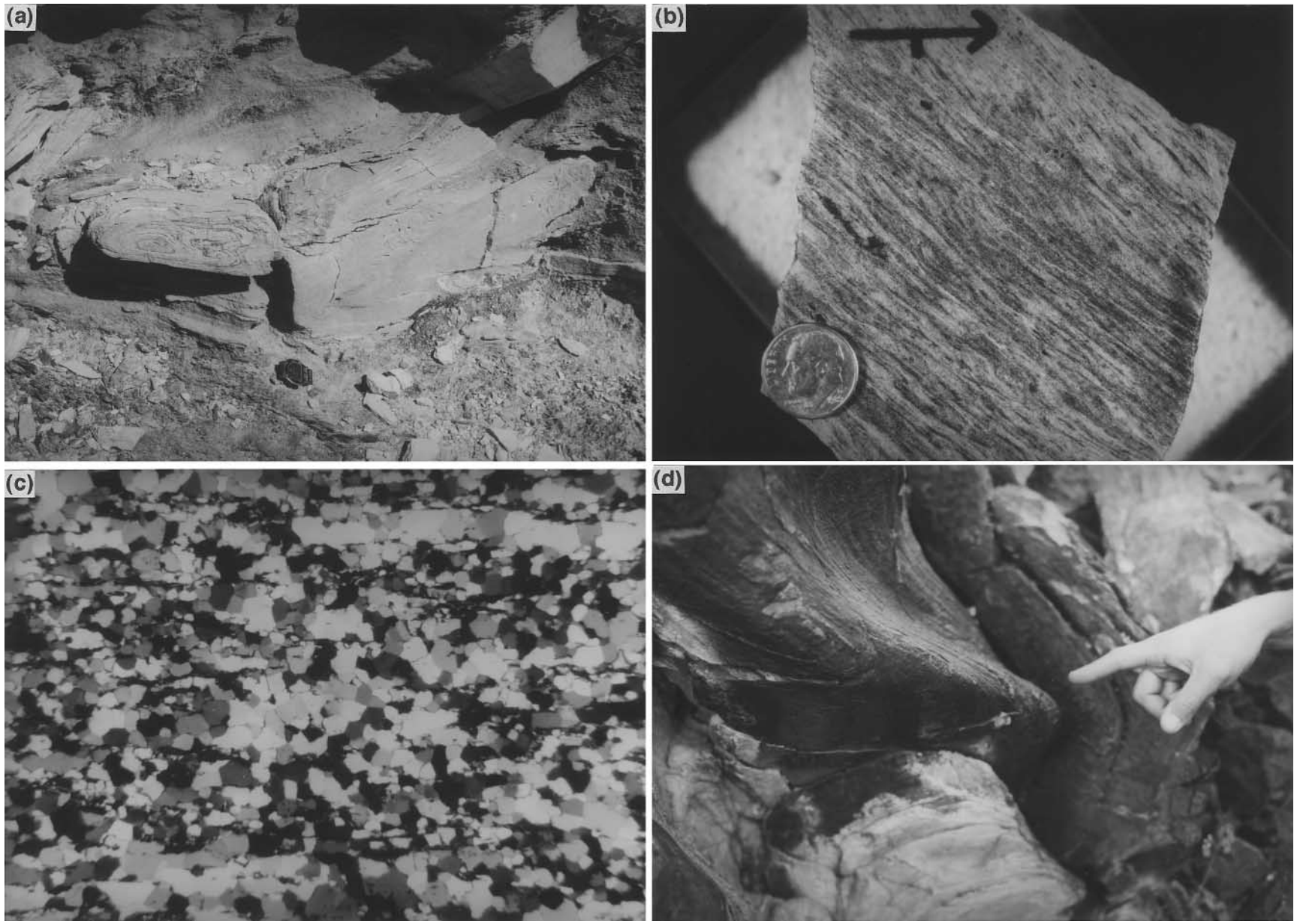

Fig. 6. (a) Three-dimensional exposure of tubular fold in Cambrian marble. Subparallel hingelines plunge gently to the northeast. Watch (4 cm diameter) in foreground for scale, view is to the northeast. (b) Polished slab of mylonitic augen gneiss from the base of the Boyer Gap shear zone. *S–C* fabric is indicative of top-to-the-south shearing (arrow oriented towards north). *S*-planes defined by mylonitic foliation that anastomoses in and out of high strain zones (*C*-surfaces). (c) Photomicrograph showing relatively high temperature rotation recrystallization of quartz in Cambrian quartzite. Field of view is 1.7 mm. (d) Three-dimensional exposure of non-cylindrical fold in Cambrian quartzite. $L_{1\times 2}$ lineation is obliquely folded across the hinge of the fold. Hingeline variation is ~60° compared to the tubular fold in (a) with hingeline variation of ~171°. View is to the west, cone-axis of the fold plunges gently to the northeast.

mation, however, does not support a decrease in temperature. Both processes, as well as the surface energy-driven grain-boundary migration, can occur at 450°C–515°C. The presence of some polygonal grains in D_2 mylonites is also consistent with upper greenschist- to lower amphibolite-facies metamorphism persisting after the cessation of southwest-directed deformation.

D_3 shear zones overprint D_2 fabrics along the Tyson thrust, Tung Hill and the Boyer Gap shear zones. Within these zones, S_2 mylonitic foliation and elongation lineation are folded on a cm- to tens of m-scale by northeast-vergent, open to tight folds (F_3) (Fig. 6d). Gently (S_{3a}) and moderately (S_{3b}) northeast-dipping spaced-cleavages transect the F_3 folds and earlier fabrics (Fig. 7a). The cleavages are defined by either pressure solution seams or 1–2 mm-wide zones of cataclasis that show normal-sense displacement (Fig. 7b). Within composite S_2/S_{3a} mylonite, kinematic indicators such as porphyroclasts with asymmetric recrystallized tails, and *S–C* fabric consistently indicate top-to-the-northeast, normal-sense shear. In metaigneous rocks, sigma-type porphyroclasts (Passchier and Simpson, 1986) are defined by aggregates of very fine-grained ($< \sim 10\ \mu m$) recrystallized feldspar that form asymmetric mantles on relict feldspar augen, indicating that migrational recrystallization (Poirer, 1985, p. 182; Tullis and Yund, 1985) was active during D_3. Some feldspar porphyroclasts are fractured, and consist of rotated fragments. In other samples, type II *S–C* mylonites (Lister and Snoke, 1984) are observed where subgrains in relict feldspar porphyroclasts and recrystallized feldspar grains form a dimensional preferred orientation that is oblique to penetrative foliation formed by compositional bands of dimensionally-aligned muscovite and fine-grained aggregates of recrystallized quartz and feldspar (Fig. 7c). The obliquely recrystallized feldspar grains formed by rotation recrystallization and show a top-to-the-northeast sense of shear. Obliquely recrystallized grains are also observed in quartz. However, they are characterized by discontinuous undulatory extinction, elongate grains with irregular grain boundaries, and core/mantle structure (Fig. 7d).

In quartzite, a dimensional preferred orientation of quartz grains define *S*-planes that are oblique to *C*-planes characterized by thin micaceous layers and ribbons of quartz. Individual quartz grains have highly irregular (serrate) grain boundaries. Large grains show discontinuous undulatory extinction and subgrains near the grain boundaries. Formation of small strain-free grains can be observed in various stages of bulge nucleation along serrate grain boundaries, a characteristic of dynamic recrystallization by grain-boundary migration (cf. Poirer, 1985, p. 182; Urai *et al.*, 1986, p. 163). Lastly, microfracturing of quartz grains occurs in 1–2 mm wide zones of cataclasis defining S_{3a} cleavage. These textures indicate that although the onset of D_3 deformation (rotation recrystallization of feldspar) occurred at temperatures greater than 450°C, most (migration recrystallization by bulge nucleation in feldspar and quartz; discontinuous undulatory extinction in quartz, microfracturing of quartz and feldspar) occurred under lower temperature ($\leq$300°C) conditions (Hirth and Tullis, 1992; Fitz Gerald and Stünitz, 1993).

The progression from crystal-plastic to brittle deformation of feldspar and quartz, preservation of strain features (subgrains and core/mantle structure) in quartz grains, presence of type II *S–C* fabrics in D_3 mylonitic rocks, and heterogeneity of D_3 strain indicates that northeast-vergent deformation developed while the rocks were cooling. The association of cooling and normal-sense displacement in composite D_2/D_3 mylonitic shear zones is characteristic of extensional deformation and exhumation.

Quartz c-axis fabrics

To further establish the relationship between shear zone fabric development and kinematic evolution, quartz *c*-axis orientations were determined for six samples of Cambrian quartzite and three samples of Triassic quartzite (Fig. 8; see Fig. 2 for locations). All samples show a strong crystallographic preferred orientation, but the resulting patterns are complex, reflecting the interplay of superposed strains.

Three samples (Fig. 8a–c) exhibit *S–C* fabric and serrate textures typical of D_3 deformation (see Fig. 7d). The two samples (Fig. 8b & c) closest to the Tung Hill shear zone exhibit crossed-girdle patterns, with sample C showing an obliquity consistent with the *S–C* fabric (defined by D_3 textures described above). Sample B, however, shows a girdle asymmetry indicating the opposite (top-to-the-southwest) sense of shear to that indicated by the *S–C* fabric in the sample. This pattern is interpreted as reflecting the polyphase history of the Tung Hill shear zone with the *c*-axis pattern recording D_2 shearing and the *S–C* fabric recording D_3 shearing. The *c*-axis pattern for sample A is less characteristic of plane strain, but is generally consistent with northeast-directed D_3 shearing.

Five other samples (Fig. 8d–h) have textures typical of D_2 deformation, with straight grain boundaries and strain-free grains of generally uniform size (see Fig. 6c), and one sample (Fig. 8i) exhibits an intermediate fabric. Sample H, collected from the upright limb of an F_2 syncline, exhibits a single girdle with an obliquity consistent with top-to-the-southwest sense of shear. All of the other five samples have non-distinctive patterns, with three (Fig. 8d, e & g) generally consistent with southwest-directed shearing. The pattern for sample F is most compatible with flattening strain, and the pattern for sample G also suggests a component of flattening. Sample I with intermediate fabrics shows a cross-girdle pattern that most likely reflects both D_2 and D_3 shear. Samples B, C, H, I, and A show Type II

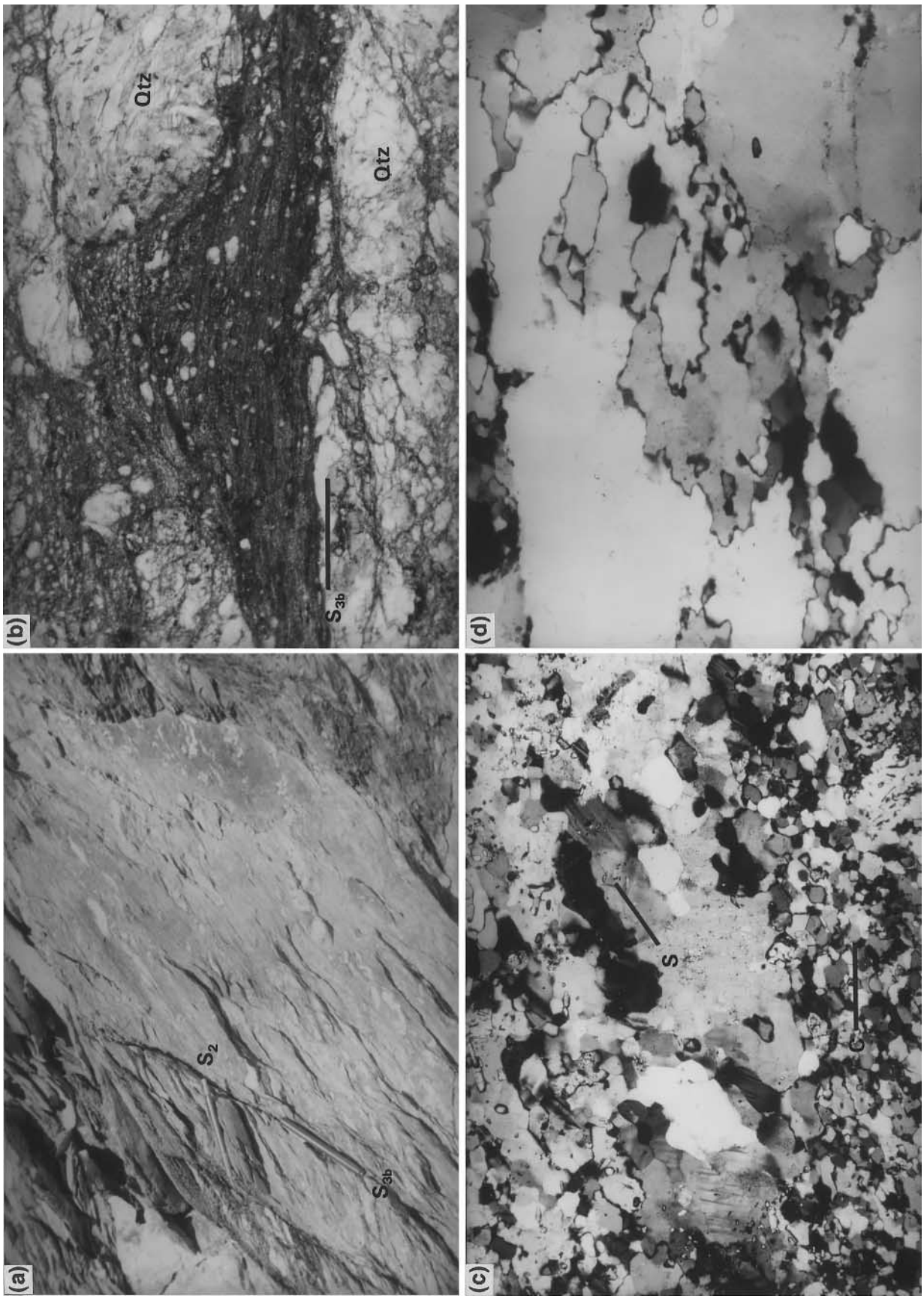

Fig. 7. (a) Northeast-dipping S_{3b} spaced-cleavage in Triassic schist near the Tyson thrust. Spaced-cleavage consistently offsets penetrative S_2 foliation in a normal-sense (down to left in photograph). View is to the southeast. (b) Photomicrograph of S_{3b} cleavage in Triassic schist, note pressure solution seams and fractured quartz grains. Plane light, field of view is 5 mm. (c) Photomicrograph of obliquely recrystallized feldspar in mylonitic augen gneiss from the Boyer Gap shear zone. Dimensional preferred orientation of subgrains and new grains defines *S*-planes that are oblique to *C*-planes defined by bands of finer-grained recrystallized quartz and feldspar. *S*–*C* geometry defines top-to-the-right (northeast) sense of shear. Field of view is 1.7 mm. (d) Photomicrograph of obliquely recrystallized quartz grains in mylonitic augen gneiss from the Tung Hill shear zone. Dimensional preferred orientation of grains defines *S*-planes that are oblique to *C*-planes defined by bands of fine-grained muscovite and recrystallized quartz. *S*–*C* geometry defines top-to-the-right (northeast) sense of shear. Field of view is 1.7 mm.

cross-girdle patterns suggesting a component of constriction.

The general lack of characteristic patterns for most samples is not surprising because the rocks have been deformed by the F_1 recumbent syncline, F_2 folds which are locally and regionally tubular (extreme sheath) folds, and D_2 and D_3 shear zones with opposite senses of motion. Local components of flattening or constriction, along with opposing senses of shear should be expected.

RELATIONSHIP BETWEEN FOLDING AND SHEAR ZONE EVOLUTION

Map relationships and fabric analysis indicate that discrete shear zones represent only a fraction of mid- to Late Cretaceous strain in the northern Dome Rock Mountains. Southwest-directed crustal shortening (D_2) is inferred to have resulted in distributed shearing and tubular-fold development on a kilometer scale in the footwall of the Tyson thrust. Sheath folds and folds with hingelines plunging directly down the dip of axial surfaces (reclined folds) are common at all scales (Fig. 6a). In metasedimentary rocks, F_1 and F_2 folds are tight to isoclinal and include class 1C, 2, and 3 fold styles (Ramsay, 1967; Fig. 9). Class 2 folds (or similar folds, Ramsay, 1967) are most commonly observed in marbles, where compositional layering appears to have had little or no mechanical influence on fold style (e.g. passive folds of Donath and Parker, 1964).

On a map scale, axial traces of F_2 major structures trend west in Boyer Gap but progressively swing into a more northwesterly orientation approaching the Dome Basin mine area (Fig. 2). The F_1/F_2 hingelines and $L_{1\times2}$ rodding lineations formed by the intersection of folded S_0/S_1 on S_2 reveals a corresponding change in orientation from an east–west trend (Boyer Gap) to a northeast-trend (Dome Basin mine) over a 2

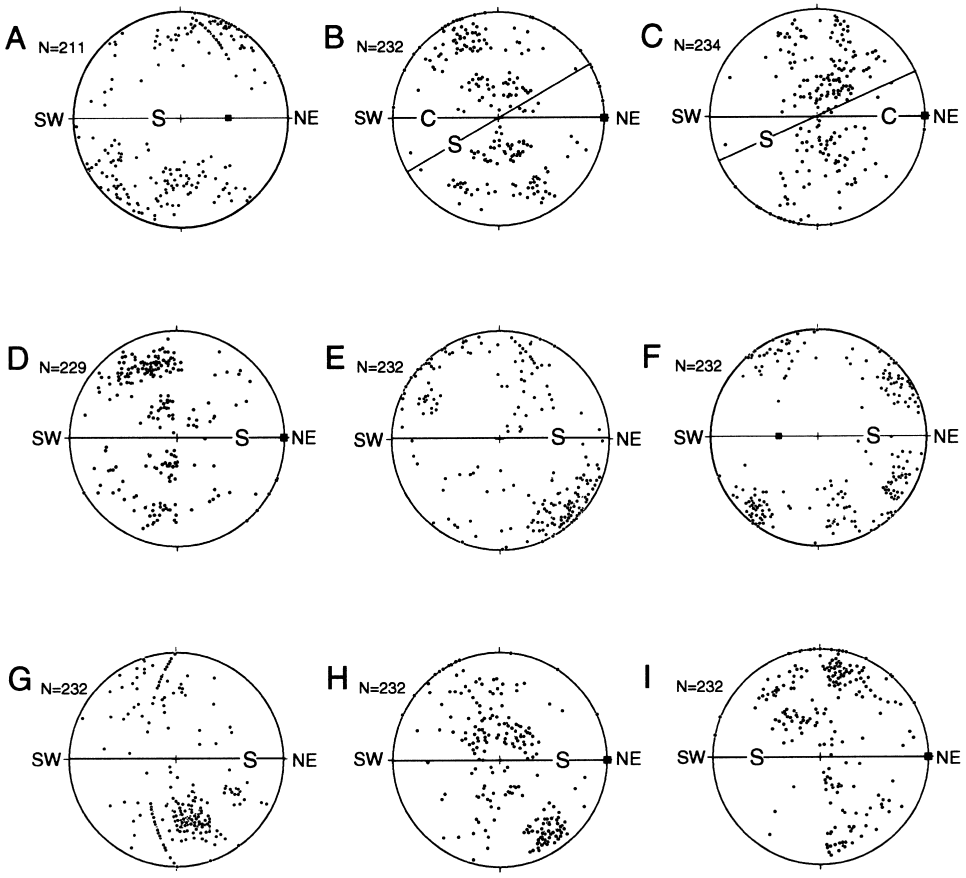

Fig. 8. Quartz *c*-axis petrofabrics for three samples (a–c) with *S–C* fabric and serrate textures typical of D_3 deformation and five samples (d–h) with straight grain boundaries and strain-free grains of generally uniform size typical of D_2 deformation. One sample (i) exhibits a fabric that is intermediate. Thin sections were cut perpendicular to penetrative foliation and parallel to lineation, where present, or parallel to the S_2 down-dip direction, where absent. For each sample, between 200–250 *c*-axis orientations were determined using a standard five-axis Universal stage and polarizing microscope. The results are displayed on equal-area plots (equatorial plane of projection) with penetrative foliation oriented east–west and vertical relative to the microscope stage; all data have been rotated into a consistent NE–SW orientation for comparison. See Fig. 2 for locations.

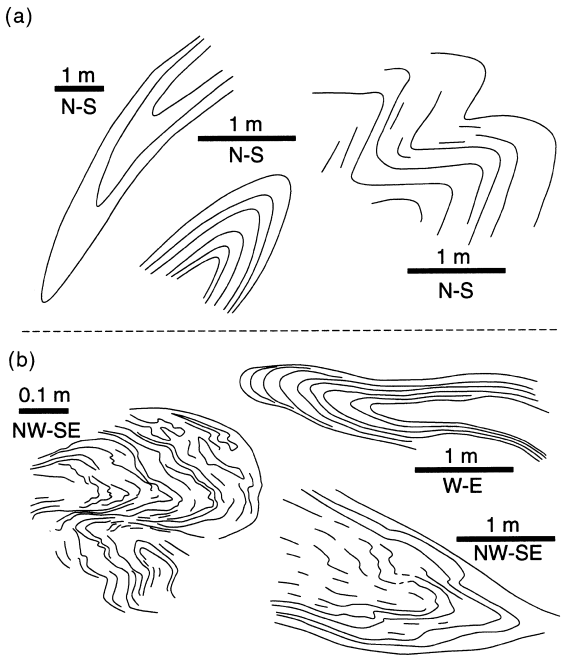

Fig. 9. Typical profiles of outcrop-scale folds of compositional layering and parallel foliation (S_0/S_1). Profiles in (a) are from Boyer Gap, where folds are typically moderately inclined, trend easterly, and show clear south- to southwest-vergence. Profiles in (b) are from Dome Basin mine area, where folds are typically recumbent, trend northeasterly, and show no clear sense of vergence.

km (horizontal) distance approaching the trace of the Tyson thrust (Fig. 2). The F_1/F_2 hingelines define a fold-hinge girdle with a point maximum parallel to the northeast-trending elongation lineation in mylonitic rocks (Fig. 2). The presence of sheath folds in outcrop at Boyer Gap with hingelines parallel to stretching lineation (Fig. 6a) suggests that other folds in the area with hingelines parallel to stretching lineation are either incompletely preserved segments of sheath folds or cylindrical F_1 folds that have become flattened and modified during D_2 shearing. These factors together have led us to interpret the arcuate pattern of F_1/F_2 fold hingelines as defining a km-scale tubular fold (extreme sheath fold, Skjernaa, 1989).

Sheath folds in shear zones are commonly described as resulting from passive amplification of initial deflections or irregularities in otherwise planar and passive layering (Cobbold and Quinquis, 1980). The initial bumps or dents are generally assumed to have main axial orientations perpendicular to the shear direction (Escher and Watterson, 1974; Ghosh and Sengupta, 1984) but can be elongate parallel to it (Skjernaa, 1989). Recent conceptual and graphical models for sheath-fold development suggest that extreme sheath folds (tubular folds) are unlikely to have formed solely by rotation from a transverse (Y) orientation into parallelism with the X-direction of the finite strain ellipse because of the unreasonably high shear strains required (Skjernaa, 1989; Mies, 1993). Tubular folds are geometrically defined as an extreme type of sheath folds with hingeline angle (β) less than 20° and ratio of long axis of the sheath (x') to the width (y) less than 1. (For symbols see Fig. 10; Skjernaa, 1989.) Skjernaa (1989) concludes that shear strains not less than $\gamma = 100$–150 are required for such a rotation during layer-parallel simple shear. Extension parallel to fold axes would probably exceed 1000% if this were the case, resulting in extremely appressed folds with z:y ratio of at least 31:1 (Skjernaa, 1980, her appendix A).

Pre-existing folds with axes oriented subparallel to the subsequent direction of tectonic transport (longitudinal folds) could, however, survive relatively high

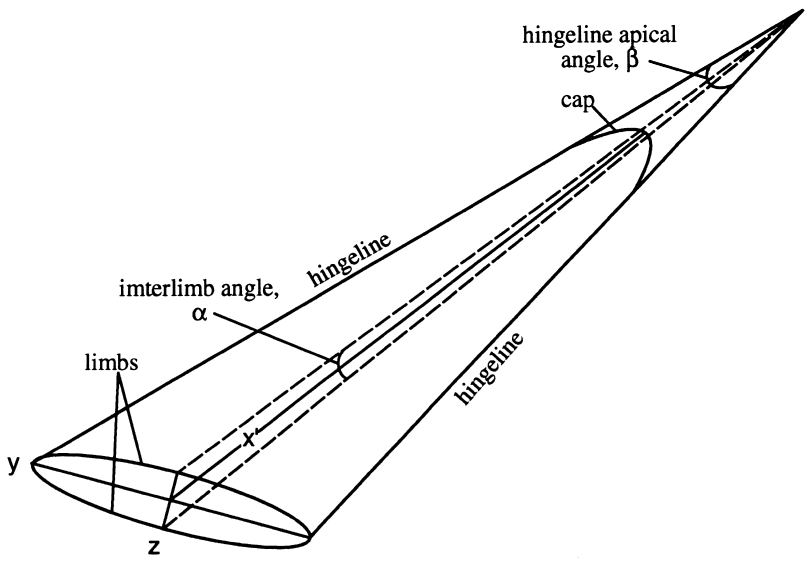

Fig. 10. Schematic illustration of tubular fold showing parameters determined for geometrical analysis. β is hingeline apical angle; z and y are the short and long dimensions of the cross section of the tube; x is the length of the tube; x' is portion of x contained within the tubular fold. After Skjernaa (1989).

shear strains (i.e. $\gamma > 10$). The new fold-axis orientations are controlled by the orientation of the already folded layers relative to the shear plane and transport direction (Skjernaa, 1989; Mies, 1993). For example, a noncylindrical upright fold deformed in a horizontal shear plane with transport sub-parallel to the fold axis would result in second fold axes subparallel to the first on the limbs, connected by a cap in the hinge that is orthogonal to the transport direction at the apex (e.g. Skjernaa, 1989, her fig. 5, p. 693).

In the northern Dome Rock Mountains, both outcrop examples and the km-scale composite structure fit the definition of a tubular fold. The tightness of F_1 and F_2 folds, however, does not generally correlate with orientation of fold hingelines relative to stretching lineation (Fig. 9), suggesting rotation of folds originally orthogonal to transport direction, and the necessary high shear strains, have not occurred. The dominant structure is a >2 km-amplitude F_1 syncline opening and younging to the northwest (Fig. 3, see trace of F_1 axial plane), consistent with the possibility that the F_1 axis was subparallel to the D_2 transport direction. Cross sections taken in three orientations across the structure (Fig. 3), coupled with the map pattern, show the F_1 major fold axis itself must curve from an east-northeast to northwest trend going from east to west in Boyer Gap and that the axial trace is folded by F_2 folds. The three-dimensional geometry of the composite F_1/F_2 nappe is illustrated in an isometric projection of cross sections A–A' and F'–F onto a block diagram with view toward the southwest (Fig. 3). The sections are linked in map view, where the outcrop pattern of Paleozoic metasedimentary rocks and F_1/F_2 axial traces in the footwall of the Tyson thrust form an arcuate shape with an apex oriented toward the southwest.

The coincidence of F_2 fold hingelines with the swing in F_1 supports the idea that the F_1 fold orientation constrained the orientation of F_2 folds. The F_2 folds, however, swing progressively into parallelism with the principal stretching direction (northeast) on the western side of Boyer Gap and northward toward the Tyson thrust. The swing of F_2 may be partially controlled by F_1 hingelines of successively younger layers in the core of the syncline, but mesoscale F_2 folds with facing toward the east and southeast are observed south of the Dome Basin mine (Fig. 2 & 3, near "F"), in a position that defines the opposite side of the tube. Extreme attenuation of stratigraphy in this location (Boettcher, 1996) is consistent with local rotation of nearly orthogonal F_2 folds into the transport direction. Thus, the larger-scale structure is a modified tubular fold in that its geometry was controlled by the preexisting F_1 major fold, but also formed in part by progressive rotation of F_2 hingelines during simple shear.

In summary, the arcuate shape and map-scale fold hingeline variation are interpreted as defining a >2 km-scale tubular fold that formed by superposition of southwest-directed, non-coaxial deformation (D_2) on the pre-existing longitudinal fold (F_1). The line perpendicular to the arc at its apex is parallel to the tectonic transport direction defined by the orientation of stretching lineation in the hangingwall of the Tyson thrust (210°), and its convex-to-the-southwest shape appears to have resulted from distributed southwest-directed deformation. Triassic metasedimentary rocks are the structurally highest rocks shown in Fig. 3 and are inferred to have been translated ~2 km to the northeast from an original position in the core of the F_1 recumbent syncline along the Tung Hill shear zone.

The evolution of the tubular fold (Fig. 11) is constrained by the present day geometry of the superposed structures described above (Fig. 3). To form the tubular fold geometry inferred, the initial major F_1 syncline must have faced north to northwest and its pre-D_2 fold axis orientation must have been oblique to the shear plane at a small clockwise angle to the direction of D_2 shearing (top-to-the-southwest, azimuth 210° from stretching lineation in shear zones; Fig. 2), with limbs at a high angle to the D_2 shear plane and the axial plane inclined. During D_2 shear zone evolution, the F_1 fold hingeline and axial plane was folded and

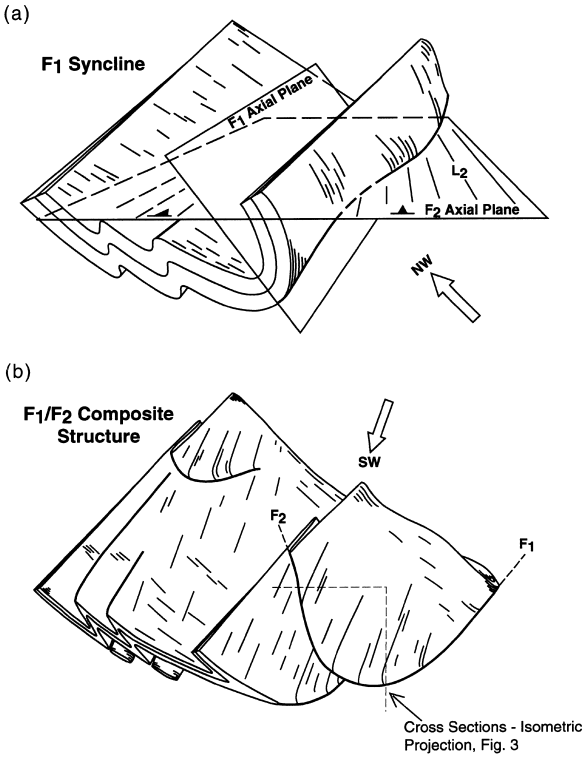

Fig. 11. Schematic illustration of superposed folds in Paleozoic metasedimentary rocks defining composite km-scale nappe in the northern Dome Rock Mountains. (a) Initial F_1 geometry relative to subsequent F_2 axial plane. (b) Superposition of southwest-directed, distributed simple shear (D_2) on pre-existing longitudinal folds (F_1) produced tubular fold geometry in footwall of Tyson thrust. Note parasitic tubular folds on lower F_1 limbs. Layers shown in illustration are representative of Cambrian Tapeats quartzite and Bright Angel schist. See text for discussion.

rotated into the shear plane. Where axial culminations are present, tubular folds can develop with a number of different geometries depending on the orientation of the shear plane (see Skjernaa, 1989, her figs 5 and 6, p. 693–694). Outcrop-scale tubular folds are interpreted to form by modification of parasitic F_1 folds in the same way as the map-scale tubular fold. Thus, the progenitors for tubular folds in the northern Dome Rock Mountains are most likely the earliest structures observed in the range, which are thought to entirely predate D_2 southwest-directed shortening (Boettcher, 1996). Extrapolating to the km-scale, the map-scale fold is interpreted to represent the modification of F_1 by D_2 shearing along the Tyson thrust and in its footwall. The initial northwest-facing F_1 fold thus predates the Tyson thrust, forming in the late Middle Jurassic, and may record northwest–southeast oriented shortening (Boettcher, 1996).

The possibility of progressive reorientation of preexisting F_1/F_2 hingelines and $L_{1\times2}$ rodding lineations during D_3 top-to-the-northeast shearing is discounted because variation in F_1/F_2 hingeline orientations occurs over a distributed area in the footwall of the Tyson thrust, independent of proximity to composite D_2/D_3 shear zones. Where $L_{1\times2}$ rodding lineations are folded obliquely across the hinges of non-cylindrical F_3 folds (Fig. 6d), the orientation of rodding lineations on the fold limbs are not parallel to stretching lineation. In addition, both open and tight F_3 folds are only mildly non-cylindrical with hingeline variations up to 60°. The intersection of folded S_2 on S_{3a} produces a lineation ($L_{2\times3}$) within composite D_2/D_3 shear zones that trends at a high angle to stretching lineation, also showing no evidence for progressive rotation into parallelism with stretching lineation.

MAGNITUDE OF MID- TO LATE CRETACEOUS DUCTILE STRAIN

In the absence of strain markers, it is difficult to quantify the magnitude of strain associated with formation of tubular folds in the northern Dome Rock Mountains. By assuming passive amplification of longitudinal folds during simple shear, however, the graphical solutions of Mies (1993, his fig. 11, p. 989) can be used to place limits on shear strain and initial fold configuration required to produce a tubular fold with a specific geometry. His solutions relate initial fold form to shear strain and tubular fold ellipticity and are modified from Skjernaa's (1989) conceptual model for tubular fold development to account for more case specific examples. Skjernaa (1989) used trigonometric calculations and equations for simple shear from Ramsay (1967) to relate the shape of a sheared dome to its original shape and to shear strain (γ). In the analysis below, we use the measured dimensions of an outcrop-scale tubular fold and the estimated tubular geometry of the map-scale F_1/F_2 fold to constrain shear strain in the footwall of the Tyson thrust using the graphical solutions of Mies (1993).

At Boyer Gap, elliptical and anvil-shaped sections are observed in marble on polished surfaces roughly orthogonal to the transport direction inferred from the orientation of stretching lineations in mylonitic rocks. A three-dimensional exposure of a sheath fold in marble, elongate parallel to stretching lineation, is defined in cross-section by similarly oriented elliptical patterns, one nested inside the other (Fig. 6a). Over the 0.25 m length of exposure, the hingelines of the sheath fold are linear and roughly parallel. Another sheath fold found as float, ~11 cm wide by ~25 cm long, is well enough preserved that its geometric configuration can be measured: β = 4.3, and at the widest end of the tube, R_{xy} = 13:1 (x, extrapolated), and R_{yz} = 4:1 (see Fig. 10 for symbols). Using the graphical solutions of Mies (1993, p. 989), and assuming an initial longitudinal fold with minor noncylindricity (hingeline variation of 20°, chosen arbitrarily), a shear strain (γ) of at least 29 is required to produce the geometry of the outcrop-scale tubular fold described above (Fig. 12a). For greater degrees of initial noncylindricity, lower values of shear strain are required.

The shear strain associated with the map-scale noncylindrical fold can be used in the same way as the outcrop example to estimate shear strain (Fig. 12b). Using the mean hingeline orientations determined from minor folds in metasedimentary rocks at opposite ends of the cap, the hingeline angle (β) is 25° (Fig. 13a). The concept of separation angle defined by Hansen (1971) can also be used to define the hingeline angle and yields a separation of about 12° (Fig. 13a). This value is considered more appropriate because mesoscale folds in the Tung Hill metasedimentary rocks (in hangingwall of Tung Hill shear zone) are oriented consistently northeast, indicating subparallelism of hingelines and stretching lineaton further away from the cap (e.g. tubular fold geometry).

The minimum length (x') of the map-scale, noncylindrical composite structure is estimated to be 2.1 km, the distance between the D_3 shear zone and northwest-trending hingelines inferred to be at the cap of the structure (Fig. 13b). The long axis (y) of an elliptical section orthogonal to x' is approximately the distance across which the hingeline variation takes place in a stratigraphic horizon, 2.1 km in this case. The short axis of the elliptical section (z) orthogonal to x' can be estimated from the thickness of the belt of Paleozoic metasedimentary rocks, about 350 m. The ratio R_{yz} is thus ~6, with $x'{:}y{:}z = > 1{:}1{:}0.17$ (Fig. 13b). Using the conservative estimate of β = 25°, a shear strain of at least 15 is required for an initially longitudinal fold with 20° hingeline variation (α_0). For the more realistic estimate of β = 12°, a shear strain of 20 is required (Fig. 12b). Integrated over the estimated

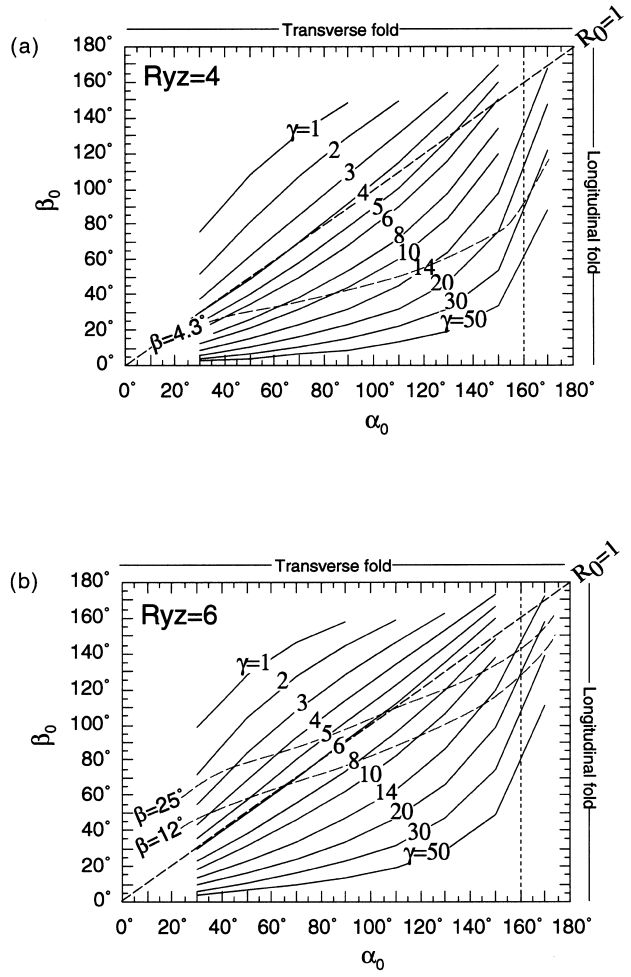

Fig. 12. Plots relating initial fold form to shear strain for outcrop-scale tubular fold (after Mies, 1993, p. 989). Curves for γ (1–50) and β = 4.3, 12, and 25 (β is hingeline apical angle of tubular fold) derived from equations (1) and (2) of Mies (1993, p. 989). In an initial structure oriented subparallel to direction of tectonic transport (longitudinal fold), α_0 is the initial hingeline apical angle (describes level of cylindricity) and β_0 is initial fold interlimb angle (note difference from α, β of final tubular fold; Fig. 9). R_0 is the ratio of β_0 to α_0; for $R_0 > 1$, the fold is termed transverse and for $R_0 < 1$ the fold is termed longitudinal (terminology of Mies, 1993). (a) Shear strain plot for cross sectional ellipse aspect ratio (R_{yz}) = 4. Assuming $\alpha_0 = 160°$, shear strain of at least 29 is required for β = 4.3° determined from hand sample of tubular fold from the eastern side of Boyer Gap. (b) Shear strain plot for cross sectional ellipse aspect ratio (R_{yz}) = 6. For $\alpha_0 = 160°$, shear strain of at least 15 is required for β = 25°; for β = 12°, shear strain of 20 is required. See Fig. 11 for further explanation and text for discussion.

350 m thickness of the tubular fold, a minimum of ~5–7 km displacement occurred across this zone.

The shear strain estimate assumes no mechanical influence of layering on fold amplification and considers a simple shear end-member case for formation of the sheath fold. Given the relative homogeneity of D_2 strain in map-scale folding of granite, quartzite, marble, and calc-silicate rocks, the overall response to strain was bulk homogeneous flow. On an outcrop scale, however, mechanical contrasts are observed, particularly in Cambrian calc-silicate rocks where boudinage and abundant veining attest to the relative strength of this rock type relative to surrounding marble. Furthermore, if a component of pure shear was involved in the deformation, the shear strain required to produce a tubular fold with the above specified dimensions would be lower. The degree of flattening cannot be quantified in the absence of strain markers, so is not incorporated into the calculation of displacement.

The above estimate of shear strain and displacement are minimum values for the northern Dome Rock

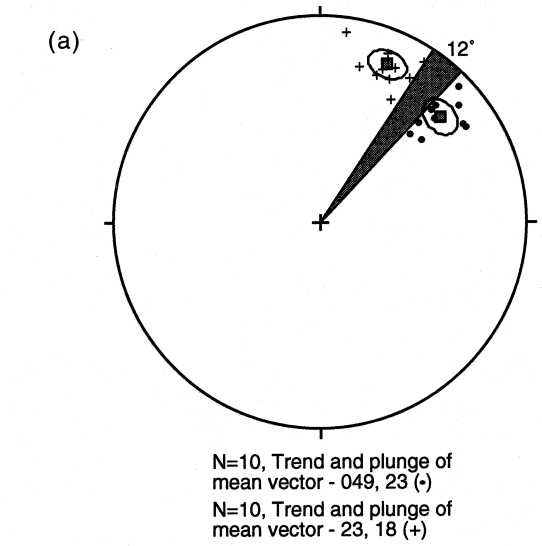

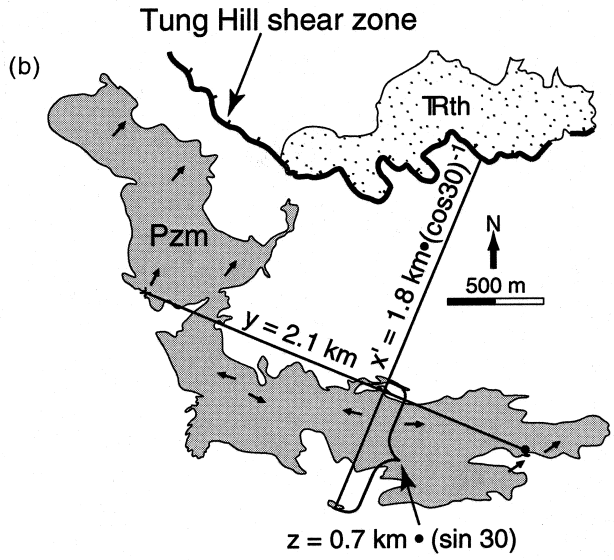

Fig. 13. (a) Trend and plunge of minor fold hingelines (•, +) at opposite ends of the exposed portion of the map-scale tubular fold. Squares denote trend and plunge of mean vector with ellipses showing 99% confidence interval. Separation angle, highlighted by grey shading, is 12°. (b) Simplified map of the study area showing representative F_1/F_2 minor fold hingelines (arrows) and Triassic metasedimentary rocks (TRth) offset from arcuate belt of Paleozoic metasedimentary rocks (Pzm) along Tung Hill shear zone. Map shows the location where minimum dimensions of map-scale tubular fold are estimated.

Mountains. The tubular fold is truncated by the Tung Hill shear zone (Fig. 3); thus the total length of the tube was not used for these estimates. In addition, the strain accommodated by the mylonitic shear zones in metaigneous rocks is not included. Values estimated in adjacent ranges are comparable. For example, Ballard (1990), inferred a shear zone geometry for the overturned limb of a range-scale southward-verging syncline in the Little Maria Mountains. By assuming an initial and final thickness of 1 km and 100 m for the cratonic section and a shear zone thickness of 2.5–5 km, displacements are estimated to be 8–16 km. In the eastern part of the Maria Belt, Laubach *et al.* (1989) report displacement of at least 10 km on the Hercules thrust system based on strain calculations and on the distance between windows into the footwall of the thrust sheet 10 km apart in the Granite Wash and Little Harquahala Mountains. The estimate of displacement across the tubular fold in the northern Dome Rock Mountains is for a narrower zone (350 m). The added displacement along the shear zones and the displacement recorded by the truncated portion of the tubular fold would increase the estimate to values similar to those for the adjacent ranges.

THERMAL EVOLUTION AND STRUCTURAL STYLE

Mid- to Late Cretaceous, basement-involved deformation in the northern Dome Rock Mountains records a transition in structural style from fold nappes to the west to more discontinuous strain involving both low-angle overthrusts and folding to the east, over a distance of ~75 km. The presence of a km-scale fold nappe and isoclinal folding of the contact between Proterozoic augen gneiss and Cambrian Tapeats quartzite (Boettcher, 1996), for example, are nearly identical to the style of deformation observed 20–40 km to the west in the Big and Little Maria Mountains. Other similarities include stratigraphy, widespread occurrence of wollastonite in the Supai Formation, and late northeast-directed ductile extensional structures. However, faults resulting from extreme attenuation of limbs during folding and the presence of a low-angle overthrust (Tyson thrust) are more characteristic of the style of deformation observed to the east in the Granite Wash and Harquahala Mountains.

Mid- to Late Cretaceous amphibolite-facies metamorphism is recorded at both ends of the Maria Belt (see Fig. 1 for locations). In the Big Maria Mountains, peak temperatures estimated from calcite–dolomite and two-feldspar thermometry range from ~430°C to ~590°C (Hoisch *et al.*, 1988). Massive wollastonite comprises 80–95% of the Supai Formation in all but the lowest-temperature (<480°C) southeastern portion of the Big Maria Mountains (Hoisch, 1987). Estimates of pressure at the time of peak metamorphism range from 2.5 to 3.5 kb and are derived from albite compositions and estimates of the minimum pressure stability for muscovite in granite (Hoisch *et al.*, 1988). In the Harquahala Mountains, at the other end of the Maria Belt, peak temperatures estimated from two-feldspar thermometry range from 470 to 570°C, with higher temperatures recorded closest to the trace of a Mesozoic thrust fault (Richard, 1988). The stability of kyanite at temperatures greater than 500°C is indicative of pressures of at least 4 kb (Holdaway, 1971), indicating that rocks in the Harquahala Mountains were buried at least as deep as rocks in the Big Maria Mountains (~12–15 km). Peak metamorphic temperatures of 450°C–515°C estimated for the northern Dome Rock Mountains (this study) are within the range of peak temperatures in the Big Maria and Harquahala Mountains but are higher than the maximum 450°C estimate of peak temperatures in the Granite Wash Mountains (Laubach, 1986).

In the northern Dome Rock Mountains, the large magnitude of shear strain distributed across the wide zone defined by the tubular fold and the continuity of the structure despite the involvement of vastly different rock types, including basement, requires low viscosities. Such behavior is usually associated with high temperatures. The variation in style along the length of the Maria Belt, however, does not simply reflect temperature variation (i.e. Harquahala Mountains) and therefore, structural depth or location relative to plutons.

Another possible strain softening mechanism suggested for parts of the Maria Belt is the presence of fluids. According to Hoisch (1987), the conversion of Supai Formation calc-silicate rocks to wollastonite in the Big and Little Maria Mountains under lower amphibolite-facies conditions requires an external control on fluid composition. Assuming no selective loss of CO_2 generated by the conversion of quartz and calcite to wollastonite, the local mineral assemblage would buffer the composition of any pre-existing fluid phase in the rock, limiting the degree to which the reaction could proceed under lower amphibolite-facies temperatures (Greenwood, 1975; Rice and Ferry, 1982; Hoisch, 1987). Infiltration of nearly pure H_2O from an external source is proposed by Hoisch (1987) to have diluted the CO_2 generated by reaction and driven the formation of wollastonite in the Big and Little Maria Mountains. Assuming an equilibrium fluid composition of $X_{H_2O} = 0.97$ and 90% wollastonite in the final rock, Hoisch (1987) calculates a minimum fluid:rock ratio of 17:1. He hypothesizes that dewatering of sediments subducted beneath the North American craton provided a renewable source of fluid sufficient to sustain a single-pass flow system.

On a cautionary note, open-system behavior resulting in CO_2 loss would eliminate the requirement for massive influx of H_2O-rich fluid. In this case, the reaction proceeds only as fast as CO_2 was removed, thus

locally maintaining a fluid in equilibrium with the surrounding rock to satisfy the condition of $X_{CO_2} < 0.03$–0.08 necessary for the reaction to proceed at 480°–590°C. Hoisch (personal communication, 1996) believes such efficient venting is unlikely given the expectation that $P_{fluid} \sim P_{total}$ for rocks with very low strength under lower amphibolite-facies metamorphic conditions. Furthermore, because CO_2 and H_2O form a supercritical fluid at temperatures greater than 265°C and are likely to be fully miscible under lower amphibolite-facies conditions (Takenouchi and Kennedy, 1964), open-system behavior driven by hydraulic gradients alone will not result in preferential removal of CO_2 from the local metamorphic system. Chemical gradients between relatively CO_2-rich fluid and pore fluids in overlying rock units could have resulted in migration of CO_2 relative to H_2O, but diffusion rates are too slow to have controlled fluid composition at the scale of tens of kilometers (e.g. Ferry, 1994). Nonetheless, without knowledge of the distribution of isotopic ratios in and adjacent to wollastonite-bearing units, the applicability of the Hoisch (1987) model for fluid infiltration remains subject to debate.

If a massive influx of water did accompany deformation, the mode and degree of infiltration would have had a significant effect on the magnitude and style of deformation observed across the Maria Belt. The pervasive fluid infiltration history suggested by Hoisch (1987) to explain the distribution of wollastonite in Big and Little Maria Mountains is consistent with the continuity of D_2 strain in the range (Ballard, 1990). In contrast, channelization of fluids into discrete D_2 ductile shear zones as proposed by Marin (1993) to explain localization of fluids within shear zones in the Granite Wash Mountains is consistent with localized strain softening causing the strain inhomogeneity in that range. In the northern Dome Rock Mountains, the widespread occurrence of wollastonite and presence of quartz, kyanite, tremolite, and actinolite veins are consistent with fluid infiltration in the footwall of the Tyson thrust during deformation. In addition, the change from high-temperature (>450°C) 'fast' grain-boundary migration in quartz to rotation recrystallization without a decrease in temperature is compatible with fluids playing an important role during deformation. Thus, a compelling hypothesis is that fluids, rather than temperature or structural level alone, controlled the style of deformation in the Maria Belt. In areas where fluid infiltration was extensive, such as the Big and Little Maria Mountains and northern Dome Rock Mountains, all rock types had similar viscosities and underwent relatively homogeneous strain. In areas where fluids were channelized, such as in the Granite Wash and Harquahala Mountains, ductile deformation was concentrated in discrete zones where the rocks were mechanically weaker than relatively dry rocks in between the major D_2 zones. Further work is needed to test this hypothesis.

Despite the variation in style, southwest-directed shortening (D_2) is the most readily correlated phase of deformation in the Maria Belt and reflects mid- to Late-Cretaceous regional contraction over a 9000 km^2 area along the truncated southwestern margin of the North American craton (Boettcher, 1996). The age of deformation is based on relationships with late Middle Jurassic and Late Cretaceous plutons (Richard, 1988; Laubach *et al.*, 1989; Boettcher, 1996), mid- to Late Cretaceous age of coarse clastic sedimentation (Tosdal and Stone, 1994), and correlation with structures outside of the Maria Belt (Boettcher, 1996).

Peak metamorphic temperatures outlasted D_2 and require an influx of heat into the crust during, and perhaps after, D_2. Assuming a stable craton geotherm of 25°C/km, rocks at ~12–15 km depth would be heated to only 300–375°C, so an additional source of heat (100–200°C) is necessary to explain the peak metamorphic temperatures in the Maria Belt. Hoisch (1987) proposes that rapid advective transfer of heat by fluids derived from dewatering of subducted sediments resulted in elevated Late Cretaceous geotherms. Additionally, mid-Cretaceous plutonism in the eastern Mojave Desert and in the root zone of the Maria Belt would have resulted in higher regional geothermal gradients. The ~92–97 Ma Teutonia batholith (DeWitt *et al.*, 1984; Miller *et al.*, 1996) and ~89 Ma metaluminous to peraluminous granitic plutons exposed in the Whipple Mountains metamorphic core complex (Anderson *et al.*, 1988) were likely emplaced during or just prior to D_2 deformation in the Maria Belt. In addition, the eastward sweep of the Cretaceous magmatic arc resulted in extensive Late Cretaceous plutonism in southeastern California and southwestern Arizona (Coney and Reynolds, 1977), promoting elevation of regional temperatures for 5–10 million years following the cessation of southwest-directed shortening. Regional cooling from temperatures greater than ~450°C is recorded by Late Cretaceous to early Tertiary $^{40}Ar/^{39}Ar$ and K/Ar ages (Martin *et al.*, 1982; Hoisch *et al.*, 1988; Richard, 1988; Knapp and Heizler, 1989; Boettcher, 1996), the oldest of which is a ~78 Ma hornblende $^{40}Ar/^{39}Ar$ age from Jurassic diorite in the Big Maria Mountains (Hoisch *et al.*, 1988). Biotite $^{40}Ar/^{39}Ar$ isochron ages from mylonitic rocks in the hangingwall and footwall of the Tyson thrust are ~48 Ma and ~55 Ma (Knapp and Heizler, 1990).

D_3, observed in parts of the Maria Belt, occurred before and after emplacement of Late Cretaceous (78–86 Ma) granites (Richard *et al.*, 1994). In the northern Dome Rock Mountains, the onset of northeast-directed motion (D_3) along the reactivated Tyson thrust predates intrusion of the Late Cretaceous (~86 Ma) Tyson Wash granite, which is undeformed where it intrudes the Tyson thrust. Recognition of S_{3a} cleavage in the northernmost exposures of the granite, however, indicates that northeast-directed motion continued after intrusion of the granite. An additional constraint

for D_3 deformation comes from the adjacent Moon Mountains. Pegmatite dikes, intruded during the latest phase of northeast-directed shearing along the Valenzuela thrust, have yielded a U–Pb age of 71.1 + 6.7 Ma (Knapp, 1989). Thus, in the northern Dome Rock Mountains, D_3 extension initiated very shortly (0–10 my) after peak temperatures ($< 515°C$) had been attained. This interpretation is consistent with the earliest D_3 structures that require temperatures of at least ~450°C and with cessation of crystal-plastic deformation of quartz in D_3 mylonites by the early Tertiary when the rocks had cooled below the closure temperature for Ar in biotite (~320°C).

The onset of extension following peak metamorphism and crustal thickening suggests release of gravitational potential energy of the thickened body as a driving force for extension. If so, D_3 northeast-directed extension can be considered a continuum of Late Cretaceous orogenesis rather than an independent tectonic event related to changing plate-boundary forces.

CONCLUSIONS

The style of mid- to Late Cretaceous ductile strain in the northern Dome Rock Mountains is transitional from the nappe-style deformation present in the Big and Little Maria Mountains to more discontinuous deformation recorded by low-angle overthrusts in the Granite Wash and Harquahala Mountains. The variation in style along the belt is interpreted to be a result of different degrees and modes of fluid infiltration rather than solely differences in structural level or temperature.

In the northern Dome Rock Mountains, penetrative structures include folds with hingelines parallel to stretching lineation and tubular folds on outcrop and map scales. Both of these types of folds are interpreted to have formed by superposition of distributed southwest-directed deformation (D_2) on pre-existing folds (F_1) with initial orientation subparallel to the direction of D_2 shearing. The major structure is a north- to northwest-facing recumbent syncline modified by D_2 shearing to form a >2 km-scale tubular fold. Applying the graphical solutions of Mies (1993), shear strains of at least 20 are required to produce the tubular fold from an initially longitudinal fold with only minor initial hingeline variation. Integrated over the 350 m thickness of the km-scale tubular fold, a minimum of 5–7 km displacement occurred across this zone in the footwall of the Tyson thrust. Northeast-vergent extensional deformation cuts the map scale tubular fold and developed while the rocks were cooling. This phase of late-orogenic extension is inferred to have developed as a manifestation of gravitationally-driven collapse of rocks mechanically weakened by fluid infiltration and upper greenschist- to lower amphibolite-facies metamorphism.

Acknowledgements—This research was supported by Geological Society of America student research awards, Sigma Xi Grant-in-Aid awards, USGS Volunteer for Science Program, and the University of Texas at Austin Geology Foundation and Department of Geological Sciences. Mark Cloos and Dick Tosdal provided significant direction, encouragement, and review during both initial development and final documentation of this research project. Stan Ballard and Richard Weiland aided in construction of geologic maps and stimulated discussion on fundamental geologic processes. Reviews by Steve Laubach, Bill Carlson, Allen Glazner, Michael Wells and Steve Ralser significantly streamlined the text. Jon Mies graciously provided graphical solutions for shear strain estimation using the different tubular fold geometries shown in Fig. 12.

REFERENCES

Anderson, J. L., Barth, A. P. and Young, E. D. (1988) Mid-crustal roots of Cordilleran metamorphic core complexes. *Geology* **16,** 366–369.

Ballard, S. N. (1990) The structural geology of the Little Maria Mountains, Riverside County, California. Unpublished Ph.D. thesis, University of California, Santa Barbara.

Boettcher, S. S. (1996) Crustal shortening, extension, and unroofing in the Dome Rock Mountains, Arizona. Unpublished Ph.D. thesis, University of Texas, Austin.

Cobbold, P. R. and Quinquis, H. (1980) Development of sheath folds in shear regimes. *Journal of Structural Geology* **2,** 119–126.

Coney, P. J. and Reynolds, S. J. (1977) Cordilleran Benioff zones. *Nature* **270,** 403–406.

DeWitt, E., Armstrong, R. L., Sutter, J. F. and Zartman, R. F. (1984) U–Th–Pb, Rb–Sr, and Ar–Ar mineral and whole-rock isotopic systematics in a metamorphosed granitic terrane, southeastern California. *Geological Society of America Bulletin* **95,** 723–739.

Donath, F. A. and Parker, R. B. (1964) Folds and folding. *Geological Society of America Bulletin* **75,** 45–62.

Dickinson, W. R., Klute, M. A. and Swift, P. N. (1986) The Bisbee basin and its bearing on late Mesozoic paleogeographic and paleotectonic relations between the Cordilleran and Caribbean regions. In *Cretaceous Stratigraphy, Western North America*, ed. P. Abbott, pp. 51–62. Pacific Section, Society of Economic Paleontologists and Mineralogists.

Escher, A. and Watterson, J. (1974) Stretching fabrics, folds, and crustal shortening. *Tectonophysics* **22,** 223–231.

Etheridge, M. A., Wall, V. J. and Cox, S. F. (1984) High fluid pressures during regional metamorphism and deformation. Implications for mass transport and deformation conditions. *Journal of Geophysical Research* **89,** 4344–4358.

Ferry, J. M. (1994) Overview of the petrologic record of fluid flow during regional metamorphism in northern New England. *American Journal of Science* **294,** 905–988.

FitzGerald, J. D. and Stünitz, H. (1993) Deformation of granitoids at low metamorphic grade I: Reactions and grain size reduction. *Tectonophysics* **221,** 299–324.

Ghosh, S. K. and Sengupta, S. (1984) Successive development of plane noncylindrical folds in progressive deformation. *Journal of Structural Geology* **6,** 703–709.

Greenwood, H. J. (1975) Buffering of pore fluids by metamorphic reactions. *American Journal of Science* **275,** 573–593.

Greenwood, H. J. (1976) Metamorphism at moderate temperatures and pressures. In *The Evolution of Crystalline Rocks*, eds D. K. Bailey and R. Macdonald, pp. 3–97. Academic Press, New York.

Hamilton, W. (1982) Structural evolution of the Big Maria Mountains, northeastern Riverside County, southeastern California. In *Mesozoic–Cenozoic Tectonics of the Lower Colorado River Region, California, Arizona, and Nevada*, eds E. G. Frost and D. L. Martin, pp. 1–27. Cordilleran Publishers, San Diego, California.

Hamilton, W. (1987) Mesozoic geology and tectonics of the Big Maria Mountains region, southeastern California. In *Mesozoic Geology of Southern Arizona and Adjacent Areas*, eds W. R. Dickinson and M. A. Klute, pp. 33–47. Arizona Geological Society Digest **18,**.

Hansen, E. (1971) *Strain Facies*. Springer-Verlag, Berlin.

Haxel, G. B., Tosdal, R. M., May, D. J. and Wright, J. E. (1984) Latest Cretaceous and early Tertiary orogenesis in south-central

Arizona: Thrust faulting, regional metamorphism, and granitic plutonism. *Geological Society of America Bulletin* **95,** 631–653.

Hirschberg, A. and Winkler, H. G. F. (1968) Stabiltätsbeziehungen zwischen Chlorit, Cordierit und Almandin bei der Metamorphose. *Contributions to Mineralogy and Petrology* **18,** 17–42.

Hirth, J. G. and Tullis, J. (1992) Dislocation creep regimes in quartz aggregates. *Journal of Structural Geology* **14,** 145–160.

Hoisch, T. D. (1987) Heat transport by fluids during Late Cretaceous regional metamorphism in the Big Maria Mountains, southeastern California. *Geological Society of America Bulletin* **98,** 549–553.

Hoisch, T. D., Miller, C. F., Heizler, M. T., Harrison, T. M. and Stoddard, E. F. (1988) Late Cretaceous regional metamorphism in southeastern California. In *Metamorphism and Crustal Evolution of the Western United States, Rubey Volume VII*, ed. W. G. Ernst, pp. 538–571. Prentice-Hall, Englewood Cliffs, New Jersey.

Holdaway, M. J. (1971) Stability of andalusite and the aluminum silicate phase diagram. *American Journal of Science* **271,** 97–131.

Howard, K. A. and John, B. E. (1987) Crustal extension along a rooted system of low-angle faults; Colorado River extensional corridor, California and Arizona. In *Continental Extensional Tectonics*, eds M. Coward, J. Dewey and P. Hancock, 299–311. Geological Society of London Special Paper **28**.

Kerrick, D. M. (1968) Experiments on the upper stability limit of pyrophyllite at 1.8 kilobars and 3.9 kilobars water pressure. *American Journal of Science* **266,** 204–214.

Knapp, J. H. (1989) Structural development, thermal evolution, and tectonic significance of a Cordilleran basement thrust terrain, Maria fold and thrust belt, west-central Arizona. Unpublished Ph.D. thesis, Massachusetts Institute of Technology, Cambridge.

Knapp, J. H. and Heizler, M. T. (1990) Thermal history of crystalline nappes of the Maria fold and thrust belt, west central Arizona. *Journal of Geophysical Research* **95,** 20049–20073.

Laubach, S. E. (1986) Polyphase deformation, thrust-induced strain and metamorphism, and Mesozoic stratigraphy of the Granite Wash Mountains, west-central Arizona. Unpublished Ph.D. thesis, University of Illinois, Urbana-Champaign.

Laubach, S. E., Reynolds, S. J., Spencer, J. E. and Marshak, S. (1989) Progressive deformation and superposed fabrics related to Cretaceous crustal underthrusting in western Arizona, U.S.A. *Journal of Structural Geology* **11,** 735–749.

Lister, G. S. and Snoke, A. W. (1984) *S–C* mylonites. *Journal of Structural Geology* **6,** 617–638.

Marin, B. A. (1993) Kinematic evolution of a ductile shear zone system, Granite Wash Mountains, west-central Arizona. Unpublished M.A. Thesis, University of Texas, Austin.

Martin, D. L., Krummenacher, D. and Frost, E. G. (1982) K–Ar geochronologic record of Mesozoic and Tertiary tectonics of the Big Maria–Little Maria–Riverside Mountains terrane. In *Mesozoic–Cenozoic Tectonics of the Lower Colorado River Region, California, Arizona, and Nevada*, eds E. G. Frost and D. L. Martin, pp. 518–550. Cordilleran Publishers, San Diego.

Mies, J. W. (1993) Structural analysis of sheath folds in the Sylacauga Marble Group, Talladega slate belt, southern Appalachians. *Journal of Structural Geology* **15,** 983–993.

Miller, D. M., Wells, M. L., Dewitt, E., Walker, J. D. and Nakata, J. K. (1996) Late Cretaceous extensional fault system across the northeastern Mojave Desert. *San Bernardino County Museum Association Quarterly* **43,** 77–84.

Passchier, C. W. and Simpson, C. (1986) Porphyroclast systems as kinematic indicators. *Journal of Structural Geology* **8,** 831–844.

Poirer, J. P. (1985) *Creep of Crystals*. Cambridge University Press, Cambridge.

Ramsay, J. G. (1967) *Folding and Fracturing of Rocks*. McGraw-Hill Book Company, London.

Reynolds, S. J., Spencer, J. E., Richard, S. M. and Laubach, S. E. (1986) Mesozoic structures in west-central Arizona. *Arizona Geological Society Digest* **16,** 35–51.

Rice, J. M. and Ferry, J. M. (1982) Buffering, infiltration, and the control of intensive variables during metamorphism. In *Characterization of Metamorphism through Mineral Equilibria*, ed. J. M. Ferry, pp. 263–326. Mineralogical Society of America Reviews in Mineralogy, **9**.

Richard, S. M. (1988) Bedrock geology of the Harquahala Mountains, west-central Arizona: Mesozoic shear zones, cooling, and Tertiary unroofing. Unpublished Ph.D. thesis, University of California, Santa Barbara.

Richard, S. M., Ballard, S. N., Boettcher, S. S., Hamilton, W. B., Hoisch, T. D. and Tosdal, R. M. (1994) Mesozoic Tectonics of the Maria Belt, west-central Arizona and southeastern California. In *Geological investigations of an active margin*, eds S. F. MaGill and T. M. Ross, pp. 272–292. San Bernardino County Museum Association, Redlands, California.

Sherrod, D. R. and Tosdal, R. M. (1991) Geologic setting and Tertiary structural evolution of southwestern Arizona and southeastern California. *Journal of Geophysical Research* **96,** 12407–12423.

Skjernaa, L. (1980) Rotation and deformation of randomly oriented planar and linear structures in progressive simple shear. *Journal of Structural Geology* **2,** 101–109.

Skjernaa, L. (1989) Tubular folds and sheath folds: definitions and conceptual models for their development, with examples from the Grapesvare area, northern Sweden. *Journal of Structural Geology* **11,** 689–703.

Spencer, J. E. and Reynolds, S. J. (1991) Tectonics of mid-Tertiary extension along a transect through west central Arizona. *Tectonics* **10,** 1204–1221.

Storre, B. and Nitsch, K.-H. (1974) Zur Stabilität von Margarit im System CaO–Al_2O_3–SiO_2–H_2O. *Contributions to Mineralogy and Petrology* **43,** 1–24.

Takenouchi, S. and Kennedy, G. C. (1964) The binary system H_2O-CO_2 at high temperatures and pressures. *American Journal of Science* **262,** 1055–1074.

Tosdal, R. M. (1990) Constraints on the tectonics of the Mule Mountains thrust system, southeast California and southwest Arizona. *Journal of Geophysical Research* **95,** 20025–20048.

Tosdal, R. M., Haxel, G. B. and Wright, J. E. (1989) Jurassic geology of the Sonoran Desert region, southern Arizona, southeastern California, and northernmost Sonora: Construction of a continental-margin magmatic arc. In *Geologic Evolution of Arizona*. pp. 397–434, eds J. P. Jenney and S. J. Reynolds Arizona Geological Society Digest, **17**.

Tosdal, R. M. and Stone, P. (1994) Stratigraphic relations and U–Pb geochronology of the Upper Cretaceous upper McCoy Mountains Formation, southwestern Arizona. *Geological Society of America Bulletin* **106,** 476–491.

Tullis, J. and Yund, R. A. (1985) Dynamic recrystallization of feldspar: A mechanism for ductile shear zone formation. *Geology* **13,** 238–241.

Urai, J. L., Means, W. D. and Lister, G. S. (1986) Dynamic recrystallization of minerals. In *Mineral and Rock Deformation: Laboratory studies*. eds B. E. Hobbs and H. C. Heard. Geophysical Monograph. pp. 161–199 American Geophysical Union, **36**.

Winkler, H. G. F. (1979) *Petrogenesis of Metamorphic Rocks*. Springer-Verlag, Berlin, Germany.

Yeats, K. J. (1985) Geology and structure of the Northern Dome Rock Mountains, La Paz County, Arizona. Unpublished M.S. thesis, University of Arizona, Tucson.